Advances in diffraction of sub-nuclear waves

Habilitation thesis document

Laurent SCHOEFFEL

CEA Saclay/Irfu-SPP, 91191 Gif-sur-Yvette, France

Contents

2

Remerciements

L'HDR est une procédure relativement longue, bien utile pour dresser un bilan d'étape sur son parcours scientifique. C'est une satisfaction qu'elle parvienne à son terme aujourd'hui. Si je me suis décidé à engager ce processus, c'est sous l'impulsion d'Ursula Bassler. Elle a su trouver les arguments pertinents pour lever mes réticences. Ensuite, Michel Davier a joué un rôle important et constructif dans la constitution du dossier. Je remercie bien évidemment les membres de mon jury qui ont accepté l'invitation : Nicole d'Hose, Michel Garçon et Etienne Augé. Merci de prendre sur votre temps. Merci beaucoup Etienne d'en avoir accepté la présidence avec autant de gentillesse. Les rapporteurs forment la dernière étape d'analyse du travail, sur dossiers ou documents. Halina Abramowicz, Wolf-Dieter Nowak et Robi Peschanski ont accepté cette charge. Merci chaleureusement à vous trois. J'ai souhaité que toutes les expériences qui sont discutées dans l'HDR, même brièvement, soient représentées. C'est ainsi une chance que cette convergence puisse avoir lieu car c'est aussi celle que j'essaie à mettre en oeuvre, avec d'autres, dans l'espace des idées.

Après tant d'années à travailler sur des analyses en physique des particules et à défendre mes résultats ici ou là, j'ai eu la chance de vivre de belles aventures scientifiques. Il est évident que le rythme imposé par les réunions de travail et les conférences confère une dynamique exogène à la production de résultats. Ce rythme trouve une résonnance dans des rencontres qui sont déterminantes. A l'occasion de cette petite note liminaire à l'HDR, je tiens à témoigner ma gratitude à celles et ceux qui ont été des compagnons de route ou bien tout simplement avec qui nous avons passé de bons moments. Je pense en particulier à la période récente avec Guillaume Jegou et Etienne Burtin et mes collègues d'ATLAS (modèle standard), Maarteen Boonekamp, Nathalie Besson et Marie Legendre. Au cours de ces dernières années, j'ai également travaillé sur des idées périphériques aux analyses de données. J'ai apprécié les discussions toujours stimulantes avec Cyrille Marquet, Gregory Soyez, Edmond Iancu et Christophe Royon, mon collègue depuis longtemps. Merci Christophe pour ton aide précieuse dans la relecture de l'HDR. Dans la thèse, je ne discute absolument pas les travaux (détecteurs et analyses) que j'ai eu l'occasion d'effectuer dans EDELWEISS pendant de nombreuses années, lors de la phase I de l'expérience. J'y ai apprécié le travail avec Xavier-Franois Navick et Michel Gros. Concernant H1, je ne peux pas être exhaustif. Il y a de nombreuses personnes que j'apprécie, tant par leur connaissance pointue de la physique que par leur gentillesse. Il y beaucoup de noms à citer, beaucoup trop pour cette petite note. Je tiens simplement à exprimer ma reconnaissance à mon compagnon de cordée au cours de mes derniers articles dans H1, publications qui constituent une partie du coeur

expérimental de l'HDR. Emmanuel Sauvan, merci pour ta grande capacité de travail, ton énergie et ton amitié. Nous avons encore une belle analyse en cours, dans un bon état d'avancement. C'est la perspective de discussions passionnantes pour l'année qui vient.

Depuis que je me suis lancé dans l'HDR, il y a un peu plus d'un an, j'ai produit sept présentations en conférences, dont trois plénières, deux articles de revue (de 92 et 65 pages), un article dans H1 et un autre en préparation. Ces sollicitations et publications témoignent de la dynamique du sujet. Avec d'autres, nous avons su creuser un chemin et rassembler une communauté autour de la physique qui est enveloppée dans l'HDR. Il est évident que cet élan doit également beaucoup à ma hiérarchie au CEA Saclay. Sans son soutien m'autorisant à partir en réunion de travail ainsi qu'en conférence, même dans les périodes budgétaires difficiles, il est certain que mon travail aurait obtenu un impact plus modeste. Merci à Ursula et Didier Vilanova pour avoir toujours accepté mes demandes dans des délais record. J'ai beaucoup de chance de travailler dans ces conditions et c'est un facteur clef de succès dans la production et publication de résultats.

A l'occasion de cette note liminaire, je m'autorise une petite introduction à l'HDR qui suit. Il y a beaucoup de styles possibles, suivant sa personnalité, ses résultats, sa position dans le milieu. J'ai choisi de présenter une monographie qui met en exergue mes travaux. Mon objectif est de dégager les deux grandes lignes de recherche que j'ai contribué à construire à travers la quinzaine de publications que je défends dans le document. Bien évidemment, c'est un choix qui m'oblige souvent à condenser les arguments afin de concentrer la discussion sur les résultats nouveaux. Le texte est donc synthétique mais il se veut toujours pédagogique en évitant autant que possible le langage technique. Comme dans tout travail écrit, il y a ainsi un balancier entre le particulier et le général et je fais souvent le choix de focaliser l'attention sur le particulier. C'est à partir de ce dernier que j'éclaire le contexte général. Par exemple, le lecteur remarquera que les GPDs ne sont pas introduites de manière formelle avec nombre de formules mais j'expose l'idée sur un cas simple (particulier) qui suit la discussion expérimentale et le formalisme s'en trouve considérablement réduit sans perte de sens. Maintenant, bonne lecture et surtout, merci d'avoir assisté à la soutenance.

1. INTRODUCTION

Understanding the fundamental structure of matter requires an understanding of how quarks and gluons are assembled to form hadrons. Of course, only when partons are the relevant degrees of freedom of the processes, which we design in the following as perturbative processes. The arrangement of quarks and gluons inside nucleons can be probed by accelerating electrons, hadrons or nuclei to precisely controlled energies, smashing them into a target nucleus and examining the final products. Two kinds of reactions can be considered. The first one consists in low momentum transfer processes with particles that are hardly affected in direction or energy by the scattering process. They provide a low resolution image of the structure, which allows to map the static, overall properties of the proton (or neutron), such as shapes, sizes, and response to externally applied forces. This is the domain of form factors. They depend on the three-momentum transfer to the system. The Fourier transformation of form factors provides a direct information on the spatial distribution of charges in the nucleon. A second type of reaction is designed to measure the population of the constituents as a function of momentum, momentum distributions, through deep inelastic scattering (DIS). It comes from higher energy processes with particles that have scored a near-direct hit on a parton inside the nucleon, providing a higher resolution probe of the nucleon structure. Such hard scattering events typically arise via electron-quark interactions or quark-antiquark annihilation processes. Nucleon can then be pictured as a large and ever-changing number of partons having appropriate distributions of momentum and spin. Many experiments in the world located at DESY (Hamburg), Jefferson Lab or JLab (Virginia), Brookhaven (New York), Fermilab (Batavia) and CERN (Geneva) can measure these processes.

Both approaches described above are complementary, but bear some drawbacks. The form factor measurements do not yield any information about the underlying dynamics of the system such as the momenta of the constituents, whereas the momentum distributions do not give any information on the spatial location of the constituents. In fact, more complete information about the microscopic structure lies in the correlation between momenta and in the correlation between momenta and transverse degrees of freedom. New results in this direction are presented in this review.

For the purpose of the exercise, we focus the discussion on our results. We put them in perspective within all the other experiments in the world, as listed above. This allows us to draw a complete picture of the field, as complete as possible regarding the frontiers of the exercise. A very first comment on the title: diffraction is a very fundamental topic in high energy physics, not necessarily linked to QCD. Major physicists of the XXth

century, active in most domains of physics, have contributed to its foundations. In this review, we present recent measurements and what we can conclude from these measurements. Modern ideas, driven by the experimental results, are of course discussed in details. Then, *advances* means *advances* since the last ten years on the front of experimental measurements and ideas that lighten these outputs. This document is a synthesis of the work of an experimentalist that has analyzed inclusive and exclusive diffraction at HERA, and contributed to define some aspects of the future of the COMPASS experiment. The contribution to new theoretical developments and the practice of models has also been the part of our activity. A seminal reference that depicts the situation in 1999 can be found in [1].

2. BASICS OF DIFFRACTION IN DIS

One of the most important experimental results from the DESY electron-proton collider HERA, working at a center of mass energy of about 300 GeV, is the observation of a significant fraction, around 10%, of large rapidity gap events in deep inelastic scattering (DIS) [2, 3]. In these events, the target proton emerges in the final state with a loss of a very small fraction ($x_{\mathbb{P}}$) of its energy-momentum.
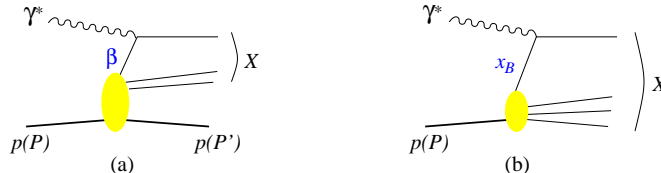

Fig. 1. Parton model diagrams for deep inelastic diffractive (a) and inclusive (b) scattering observed at lepton-proton collider HERA. The variable β is the momentum fraction of the struck quark with respect to $P - P'$, and the Bjorken variable x_{Bj} its momentum fraction with respect to P.

In Fig. 1(a), we present this event topology, $\gamma^* p \rightarrow X \; p'$, where the virtual photon γ^* probes the proton structure and originates from the electron. Then, the final hadronic state X and the scattered proton are well separated in space (or rapidity) and a gap in rapidity can be observed in the event with no particle produced between X and the scattered proton. In the standard QCD description of DIS, such events are not expected in such an abundance since large gaps are exponentially suppressed due to color strings formed between the proton remnant and scattered partons (see Fig. 1(b)). The theoretical description of such processes, also called diffractive processes, is challenging since it must combine perturbative QCD effects of hard scattering with non perturbative phenomena of rapidity gap forma-

tion. The name diffraction in high-energy particle physics originates from the analogy between optics and nuclear high-energy scattering. In the Born approximation the equation for hadron-hadron elastic scattering amplitude can be derived from the scattering of a plane wave passing through and around an absorbing disk, resulting in an optic-like diffraction pattern for hadron scattering. The quantum numbers of the initial beam particles are conserved during the reaction and then the diffractive system is well separated in rapidity from the scattered hadron.

The early discovery of large rapidity gap events at HERA [2] has led to a renaissance of the physics of diffractive scattering in an entirely new domain, in which the large momentum transfer provides a hard scale. This observation has then revived the rapidity gap physics with hard triggers, as large-$p_\perp$ jets, at the proton-antiproton collider Tevatron, currently working at a center of mass energy of about 2 TeV (see Fig. 2).
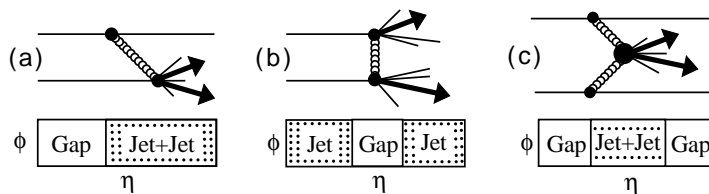
Fig. 2. Schematic diagrams of topologies representative of hard diffractive processes studied by the proton-antiproton collider Tevatron.

Whether the existence of such hard scales makes the diffractive processes tractable within perturbative QCD or not has been a subject of intense theoretical and experimental research during the past decade. Using the standard vocable, the vacuum/colorless exchange involved in the diffractive interaction is called Pomeron in this review.

3. Observation of diffractive events at HERA

Let us start by giving a real example of a diffractive event in HERA experiments. See Fig. 3, which is the (exact) experimental reproduction of Fig. 1. A typical DIS event as shown in the upper plot of Fig. 3 is $ep \rightarrow eX$ where electron and jets are produced in the final state. The electron is scattered in the backward detector[1] (right of the figure) whereas some hadronic activity is present in the forward region of the detector. The proton is thus completely destroyed and the interaction leads to jets and proton remnants directly observable in the detector. The fact that much

---

[1] At HERA, the backward (resp. forward) directions are defined as the direction of the outgoing electron (resp. proton).

energy is observed in the forward region is due to color exchange between the scattered jet and the proton remnants. However, for events that we have called diffractive, the situation is completely different. Such events appear like the one shown in the bottom of Fig. 3. The electron is still present in the backward detector, there is still some hadronic activity (jets) in the LAr calorimeter, but no energy above noise level is deposited in the forward part of the detectors. In other words, there is no color exchange between the proton and the produced jets. The reaction can then be written as $ep \to epX$.

From this observation of diffractive events, the inclusive diffractive cross section has been measured at HERA by H1 and ZEUS experiments over a wide kinematic range [2, 3], as illustrated in Fig. 4. We notice that the diffractive cross section, $ep \to epX$, shows a hard dependence in the center-of-mass energy of the γ^*p system W. Namely, we measure a W dependence of the form $\sim W^{0.6}$ for the diffractive cross section, compatible with the dependence expected for a hard process. This first observation is fundamental and allows further studies of the diffractive process in the context of perturbative QCD. The experimental selection of diffractive events is already a challenge but the discovery that these events build a hard scattering process is a surprise and makes the strong impact of HERA data into the field. Indeed, the extent to which diffraction, even in the presence of a hard scale, is a hard process, was rather unclear before HERA data. This has changed since then, with the arrival of accurate HERA data on diffraction in ep scattering and the realization that diffraction (measured to be a hard process) in DIS can be described in close analogy with inclusive DIS [3]. This is also confirmed in Fig. 6 and 7, where the ratio of diffractive to DIS cross sections is shown. This ratio is found to depend weakly on the Bjorken variable x_{Bj} (or W) at fixed values of the photon virtuality Q^2. Thus, we can conclude that diffraction in DIS is a leading twist effect with logarithmic scaling violation in Q^2, as for standard DIS. We discuss these results much further in the next sections.

4. DIFFRACTION AND THE RESOLVED POMERON MODEL

Several theoretical formulations have been proposed to describe the diffractive exchange. The purpose is to describe the *blob* displayed in Fig. 1 in a quantitative way, leading to a proper description of data shown in Fig. 4. Among the most popular models, the one based on a point-like structure of the Pomeron assumes that the exchanged object, the Pomeron, is a color-singlet quasi-particle whose structure is probed in the reaction [4, 5]. In this approach, diffractive parton distribution functions (diffractive PDFs) are derived from the diffractive DIS cross sections in the same way
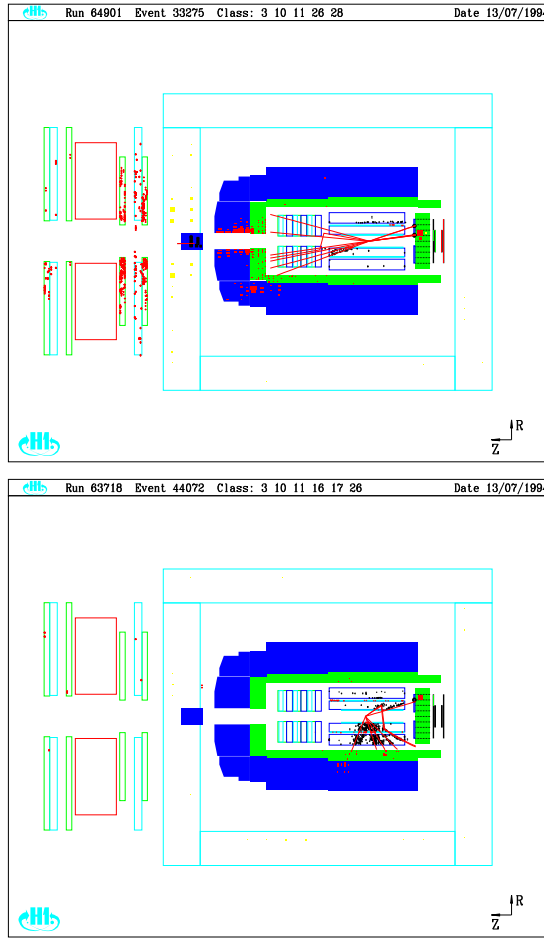
Fig. 3. Usual (top) and diffractive (bottom) events in the H1 experiment at HERA. For a diffractive event, no hadronic activity is visible in the proton fragmentation region, as the proton remains intact in the diffractive process. On the contrary, for a standard DIS event, the proton is destroyed in the reaction and the flow of hadronic clusters is clearly visible in the proton fragmentation region (+z direction, i.e. forward part of the detector).

as standard PDFs are extracted from DIS measurements. It assumes also that a certain flux of Pomeron is emitted off the proton, depending on the variable $x_{\mathbb{P}}$, the fraction of the longitudinal momentum of the proton lost during the interaction. The partonic structure of the Pomeron is probed
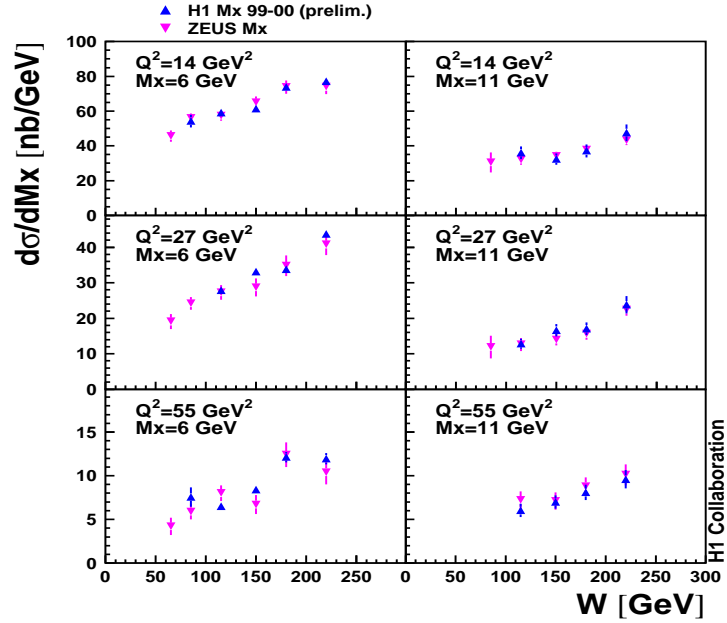
Fig. 4. The cross section of the diffractive process $\gamma^* p \to p' X$, differential in the mass of the diffractively produced hadronic system X (M_X), is presented as a function of the center-of-mass energy of the $\gamma^* p$ system W. Measurements at different values of the virtuality Q^2 of the exchanged photon are displayed.
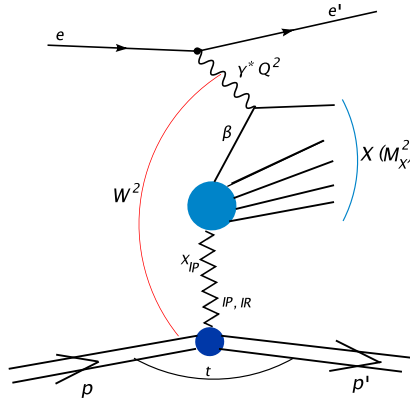

Fig. 5. Diffractive kinematics.

during the diffractive exchange [4, 5]. In Fig. 5, we illustrate this factorization property and remind the notations for the kinematic variables used in this paper, as the virtuality Q^2 of the exchanged photon, the center-of-
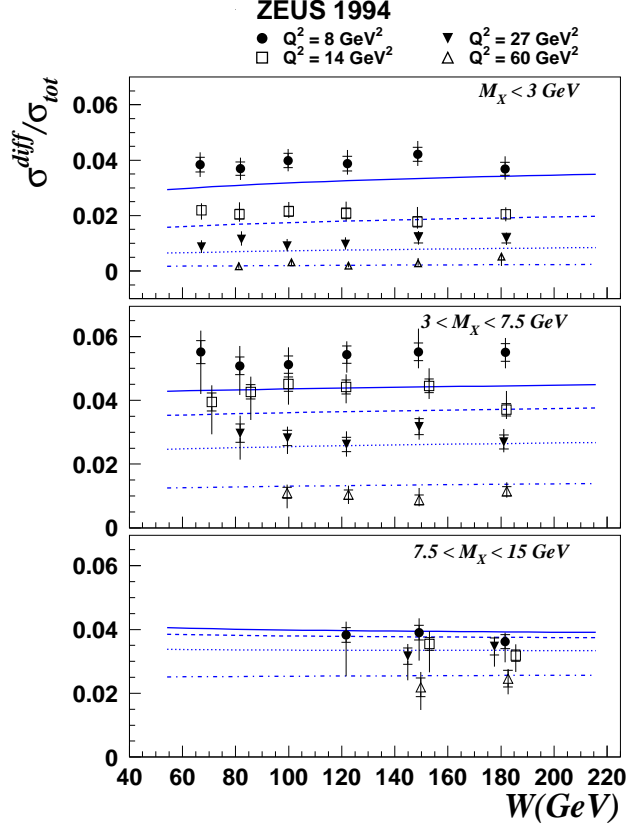
Fig. 6. Ratio of the diffractive versus the inclusive cross sections as a function of W for different values of Q^2 and the diffractive mass M_X.

mass energy of the $\gamma^* p$ system W and M_X the mass of the diffractively produced hadronic system X. It follows that the Bjorken variable x_{Bj} verifies $x_{Bj} \simeq Q^2/W^2$ in the low x_{Bj} kinematic domain of the H1 and ZEUS measurements ($x_{Bj} < 0.01$). Also, the Lorentz invariant variable β defined in Fig. 1 is equal to $x_{Bj}/x_{\mathbb{P}}$ and can be interpreted as the fraction of longitudinal momentum of the struck parton in the (resolved) Pomeron.

Because the short-distance cross section ($\gamma^* - q$) of hard diffractive DIS is identical to inclusive DIS, the evolution of the diffractive parton distributions follows the same equations as ordinary parton distributions. It follows that the characteristics of diffraction are entirely contained in the input
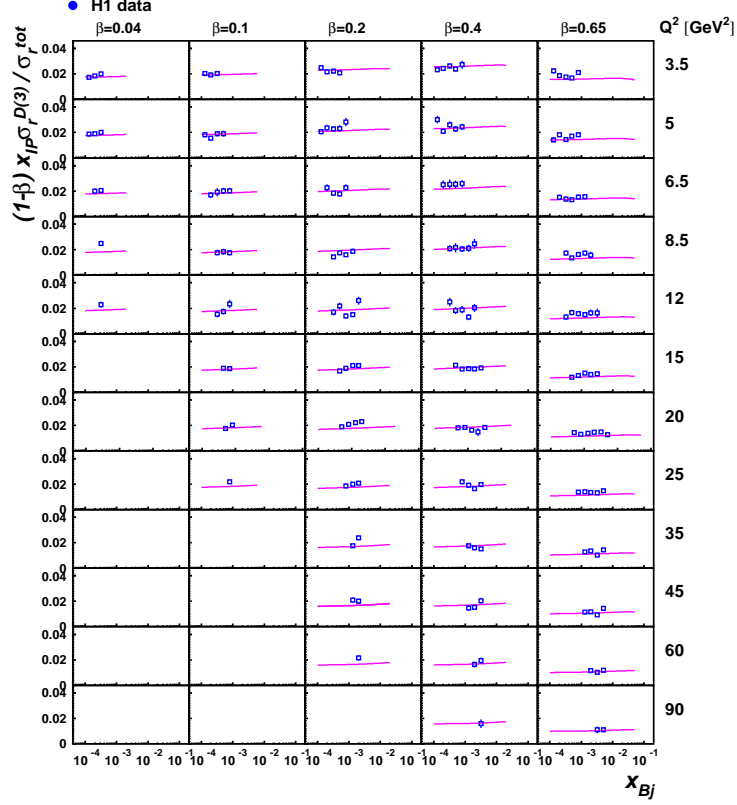
Fig. 7. Ratio of the diffractive versus total cross sections, as a function of x_{Bj}, derived from H1 data for different values of Q^2 and β. A constant ratio of about 0.02 (2%) is observed for each bin of measurements. If we add up the five bins in β (for the bulk of the Q^2 domain), we find immediately the average factor of 10%. It gives the fraction of diffractive events on the total DIS sample (see text). In this plot, the notation $\sigma_r^{D(3)}$ holds for the reduced cross section, defined as follows: $\frac{d^3\sigma^{ep \to eXp}}{dx_{\mathbb{P}}\ dx\ dQ^2} = \frac{4\pi\alpha^2}{xQ^4}(1 - y + \frac{y^2}{2})\sigma_r^{D(3)}$.

distributions at a given scale. It is therefore interesting to model these distributions.

In Fig. 8 we present the result for diffractive PDFs (quark singlet and gluon densities), obtained using the most recent inclusive diffractive cross sections presented in Ref. [3]. For each experiment (H1 and ZEUS), we include measurements derived from Large Rapidity Gap (LRG) events in

the QCD analysis. We follow the procedure described in Ref. [6], with previous ZEUS data. Note also that in all QCD fits, we let the global relative normalization of the data set as a free parameter (with respect to H1 LRG sample) [6]. The typical uncertainties for the diffractive PDFs in Fig. 8 ranges from 5% to 10% for the singlet density and from 10% to 25% for the gluon distribution, with 25% at large z (which corresponds to large β for quarks) [6]. Similar results have been obtained by the H1 collaboration [3] (see Fig. 9).
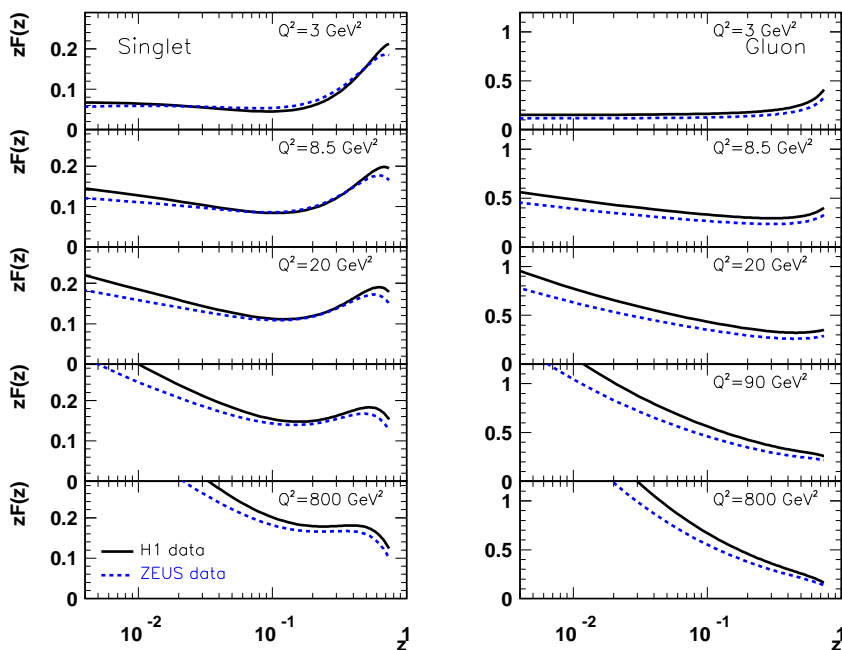

Fig. 8. Singlet and gluon distributions of the Pomeron as a function of z, the fractional momentum of the Pomeron carried by the struck parton, derived from QCD fits on H1 and ZEUS inclusive diffractive data (LRG)[3]. The parton densities are normalized to represent $x_{\mathbb{P}}$ times the true parton densities multiplied by the flux factor at $x_{\mathbb{P}} = 0.003$ [6]. A good agreement is observed between both diffractive PDFs, which indicates that the underlying QCD dynamics derived in both experiments is similar.

In order to analyze in more detail the large z behavior of the gluon distribution $zG(z, Q^2 = Q_0^2)$ and give a quantitative estimate of the systematic error related to our parameterizations, we consider the possibility to change
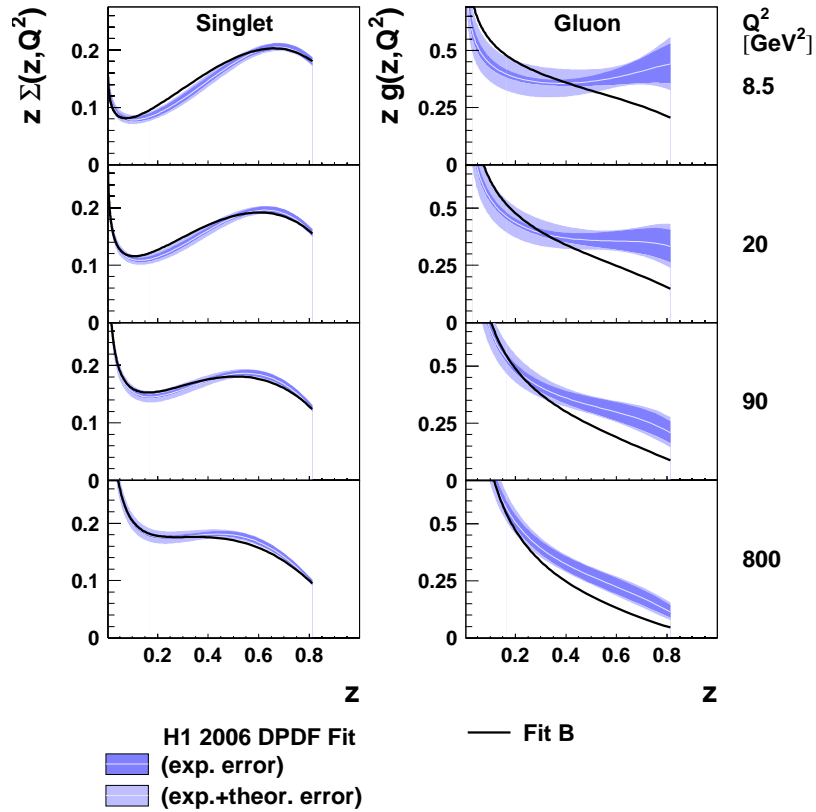
Fig. 9. Diffractive PDFs extracted by the H1 collaboration [3].

the gluon parameterization by a multiplicative factor $(1-z)^\nu$ (see Ref. [6]). If we include this multiplicative factor $(1-z)^\nu$ in the QCD analysis, we derive a value of $\nu = 0.0 \pm 0.5$ (using the most recent data). Thus, we have to consider variations of ν in the interval ± 0.5 in order to allow for the still large uncertainty of the gluon distribution (mainly at large z values). The understanding of the large z behavior is of essential interest for any predictions at the Tevatron or LHC in central dijets production (see below). In particular, a proper determination of the uncertainty in this domain of momentum is necessary and the method we propose in Ref. [6] is a quantitative estimate, that can be propagated easily to other measurements.

Of course, several checks need to be done to analyze the stability of the

QCD fits procedure [6]. We present two of them below:

- We have checked the dependence of the DPDFs on variations of the starting scale Q_0^2 in Fig. 10 (left). Very small changes are observed while changing the starting scale form 3 to 1.75 GeV^2.

- We have checked the fit stability by changing the cut on Q_{min}^2, the lowest value of Q^2 of data to be included in the fit. The results are given in Fig. 10 (right), where we show the results of the fits after applying a cut on Q_{min}^2 of 4.5, 8.5 and 12 GeV^2. Differences are noticeable at small β but well within the fit uncertainties. No systematic behavior is observed within Q_{min}^2 variations.

Then, an important conclusion is the prediction for the longitudinal diffractive structure function. In Fig. 11 we display this function with respect to its dependence in β (Fig. 11 (a)) and the ratio R of the longitudinal to the transverse components of the diffractive structure function (Fig. 11 (b)).
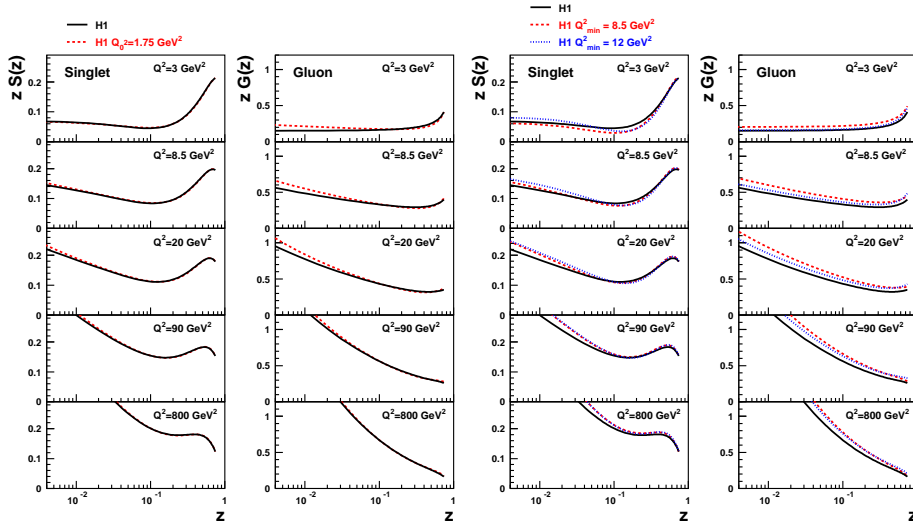

Fig. 10. Left: Singlet and gluon distributions of the Pomeron as a function of z, the fractional momentum of the Pomeron carried by the struck parton, derived from QCD fits on H1 data. Results are presented with $Q_0^2 = 3$ GeV^2 (full lines) and $Q_0^2 = 1.75$ GeV^2 (dashed lines). Normalization follows the convention explained in Fig. 8. Right: Singlet and gluon distributions of the Pomeron as a function of z derived from QCD fits on H1 data. Results are presented with $Q_{min}^2 = 4.5$ GeV^2 (full lines), $Q_{min}^2 = 8.5$ GeV^2 (dashed lines) and $Q_{min}^2 = 12$ GeV^2 (dotted lines).
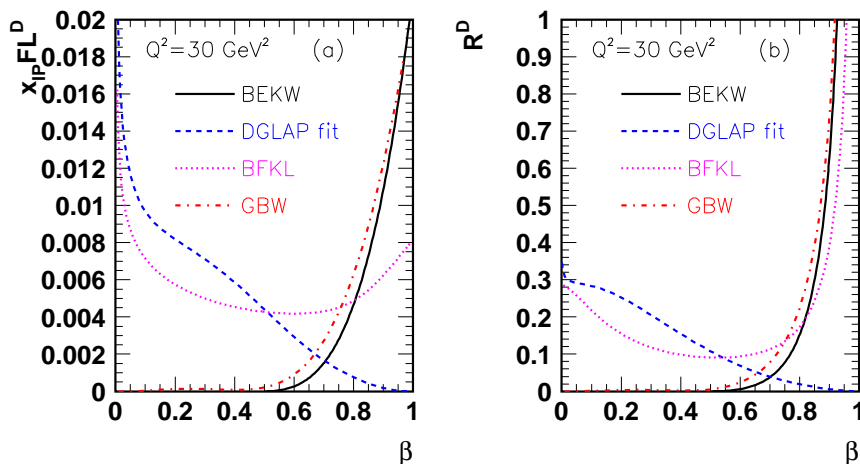
Fig. 11. Predictions for $x_{\mathbb{P}} F_L^D$ and $R^D = \frac{F_L^D}{F_2^D - F_L^D}$ as a function of β at $Q^2 = 30$ GeV^2 and $x_{\mathbb{P}} = 10^{-3}$ [6]. The dashed line prediction refers to the diffractive PDFs analysis discussed in this part. Note that the longitudinal structure function F_L^D is directly related to the the reduced diffractive cross section, presented in Fig. 7: $\sigma_r^{D(3)} = F_2^{D(3)} - \frac{y^2}{1+(1-y)^2} F_L^{D(3)}$. Other curves represent dipole model calculations (see next sections).

The resolved Pomeron model gives a good description of HERA data but fails to describe the Tevatron results [7, 8]. This effect is illustrated in Fig. 12. We note a large discrepancy both in shape and normalization between HERA predictions and CDF data, clearly showing what we can call factorization breaking. Indeed, the situation is more complex in a hadronic environment. Some underlying interactions can occur during the p-$\bar{p}$ collision, which break the gap in rapidity produced in the diffractive process. That's what we observe in Fig. 12.

Another difference between diffraction at HERA and the Tevatron is that diffraction at the Tevatron can occur not only on either p or $\bar{p}$ side as at HERA, but also on both sides. The former case is called single diffraction (or single Pomeron exchange) and the other one, double diffraction (or double Pomeron exchange). In the same way as we have defined the kinematic variables $x_{\mathbb{P}}$ and β at HERA, we define $\xi_{1,2}$ as the fractional momenta loses of protons and $\beta_{1,2}$, the fractions of the Pomeron momentum carried by the
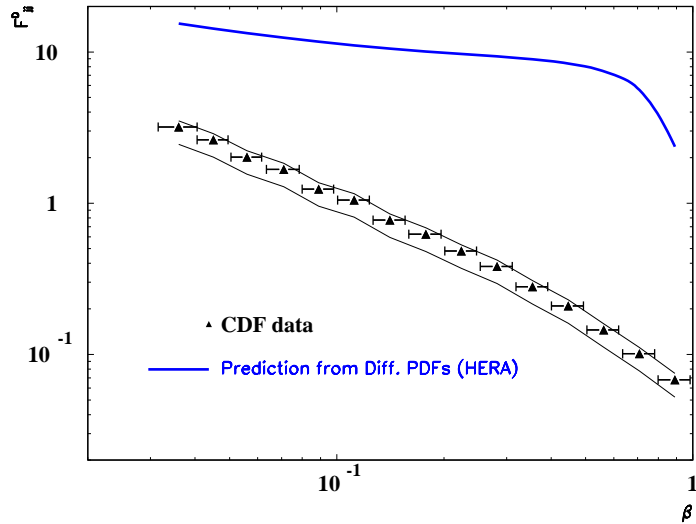
Fig. 12. Comparison between the CDF measurements ($Q^2 = 75$ GeV^2, $0.035 < \xi < 0.095$ and $|t| < 1$ GeV^2) of diffractive structure function (black points) with the expectation of the HERA (using first H1 diffractive data) diffractive PDFs [6]. The large discrepancy both in shape and normalization between HERA predictions and CDF data illustrates the breaking of factorization at the Tevatron. Using the most recent measurements in QCD fits (and diffractive PDFs extraction) does not change this conclusion.

interacting partons. The produced diffractive mass is equal to $M^2 = s\xi_1$ for single diffractive events and to $M^2 = s\xi_1\xi_2$ for double Pomeron exchange, where $\sqrt{s}$ is the energy of the reaction in the center of mass frame. The size of the rapidity gap is then of the order of $\Delta\eta \sim \log 1/\xi_{1,2}$.

The CDF collaboration has measured the so-called dijet mass fraction (DMF) in dijet events when the antiproton is tagged in roman pot detectors and when there is a rapidity gap on the proton side to ensure that the event corresponds to a double Pomeron exchange. The measured observable R_{jj} is defined as the ratio of the mass carried by the two jets divided by the total diffractive mass. The DMF turns out to be a very appropriate observable for identifying the exclusive production, which would manifest itself as an excess of the events towards $R_{jj} \sim 1$. Indeed, for exclusive events, the dijet mass is essentially equal to the mass of the central system because no Pomeron remnant is present. Then, for exclusive events, the DMF is
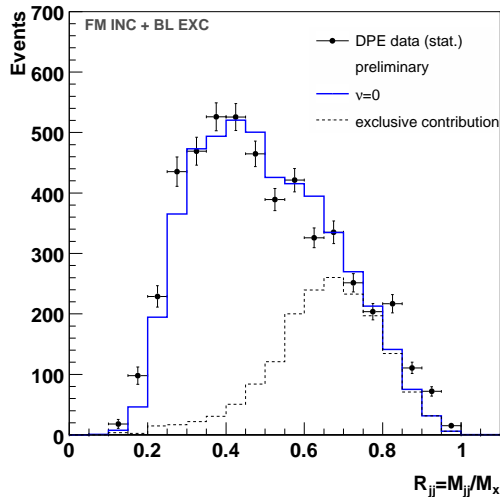
Fig. 13. Dijet mass fraction for jets $p_T > 10\,\text{GeV}$. The data are compared to the sum of inclusive and exclusive predictions. The diffractive PDFs derived from H1 data have been used together with the survival gap probability measured with single diffractive events at Tevatron.

1 at generator level and can be smeared out towards lower values taking into account the detector resolutions. If we focus the attention on the large R_{jj} part ($R_{jj} \sim 1$), the advantage of the DMF is that one can focus on the shape of the distribution and let the absolute normalization of the predictions as free parameters (in a first step). Results are shown in Fig. 13 with expectations described in Ref. [6]. These predictions are displayed for inclusive double Pomeron exchange events, where remnants are still present in the reaction and then R_{jj} is lower than unity. A specific model is also displayed in Fig. 13 for exclusive events. We observe a good agreement when both contributions, inclusive and exclusive, are taken into account. In fact, a prediction with inclusive simulation only is not sufficient to describe the present data, and shows a clear deficit of events towards high values of the DMF, where exclusive events are supposed to occur. Even taking into account the full uncertainty at large z for the diffractive gluon distribution, it is not possible to recover the observed shape of the DMF at large R_{jj} [6]. This part of the DMF is however properly described by the exclusive contribution, once normalized to fit the histogram. It is a first evidence that exclusive events could contribute at the Tevatron [6].

The great interest of studying such exclusive dijet events is that it opens

the possibility to analyze the production of heavy objects in double Pomeron exchange at the LHC [8, 9]. Schematic views of non diffractive, inclusive double Pomeron exchange, exclusive diffractive events at the Tevatron or the LHC are displayed in Fig. 15. The third class of processes in the lower left of Fig. 15, namely the exclusive diffractive production, follows directly from the discussion above. In such events, the full energy is used to produce the heavy object (like dijets, diphotons or why not, Higgs boson) and no energy is lost in Pomeron remnants. In particular, the production of a Higgs boson in such a topology could be interesting as the event would be very clean : both protons escape and are detected in Roman pots, two large rapidity gaps on both sides and the central production of the Higgs boson, leading to some decay products well isolated in the detector. The major advantage of such events is that the resolution on the mass of the produced object can be determined with a high resolution from the measurement of the proton momentum loses, using the relation $M^2 = s\xi_1\xi_2$. A potential signal, accessible in a mass distribution, is then not washed out by the lower resolution when using central detectors, rather than forward Roman pots to measure ξ_1 and ξ_2. Of course, this is an incredible experimental challenge to trigger on such events in the LHC hadronic environment. Timing resolution detectors must be used, with resolution of the order of a few nano-seconds [8, 9].

On the other hand, we must not forget the metrology point of view. It could also be possible to probe the high z diffractive gluon density at the LHC through the measurement of the dijet mass fraction (or the total diffractive mass). In Fig. 14, we present the dijet mass fraction using the shape of diffractive gluon distribution derived from HERA data [6]. Following the previous discussion, the sensitivity to the uncertainty on the gluon distribution at high z is indicated on that figure by multiplying the gluon distribution by $(1 - z)^\nu$, which enhances or decreases the high z gluon distribution. At the moment, using Tevatron data, it is not yet possible to check on data the effect displayed in Fig. 14, as essentially the normalization is not known in Fig. 13. It is not a problem for an analysis focused on the large DMF spectrum, as discussed above, but it is severely limiting the better understanding of diffractive PDFs. However, as we have shown, it is quite important to be able in the future to constrain this distribution since it is a direct background to an eventual exclusive signal at high z. At the LHC, it will be certainly possible to provide better constraints on the high z gluon density using the DMF or higher mass objects, for instance in $t\bar{t}$ inclusive diffractive production [6]. This could be a first step (improving the present knowledge of diffractive PFDs) before further exploratory analysis.
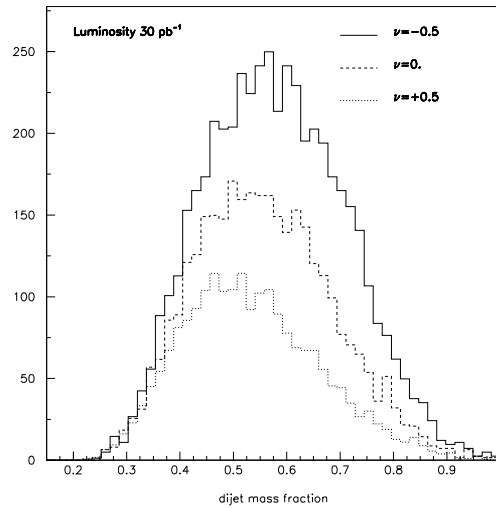
Fig. 14. Results for Dijet mass fraction at the LHC using diffractive parton distributions determined from HERA data (see Ref. [6]), as a function of the high-z tail. The high z component of the diffractive gluon density is modified by a factor $(1 - z)^{\pm \nu}$ in order to show the dependence of the dijet mass fraction on this large z shape for zG.
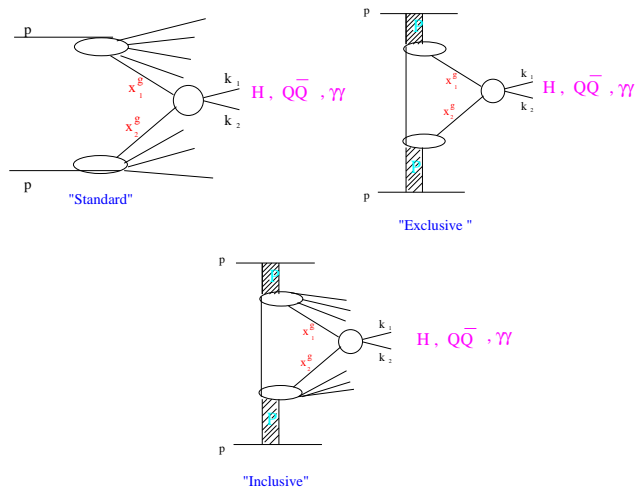

Fig. 15. Scheme of non diffractive, inclusive double Pomeron exchange and exclusive events at the Tevatron or LHC

5. Diffraction and the dipole model

The physical picture of hard diffraction is interesting in the proton rest frame and reminiscent of the aligned jet model. In the proton rest frame, at small x_{Bj}, the virtual photon splits into a $q\bar{q}$ pair long before it hits the proton [10, 11, 12, 13]. The $q\bar{q}$ wave-function of the virtual photon suppresses configurations in which one of the quarks carries almost all momentum. In fact, these configurations are the ones that give rise to a large diffractive cross section. Just because the wave-function suppression is compensated by the large cross section for the scattering of a $q\bar{q}$ pair of hadronic transverse size off the proton. The harder of the two quarks is essentially a spectator to diffractive scattering. The scattering of the softer quark off the proton is non-perturbative and cannot be described by exchange of a finite number of gluons. Hence there is an unsuppressed probability that the softer quark leaves the proton intact. This explains simply the leading twist nature of hard diffraction. The details of the scattering of the softer quark off the proton are encoded in the diffractive quark distribution. In a similar way, the $q\bar{q}g$ configuration in the virtual photon, in which the $q\bar{q}$ pair carries almost all momentum, gives rise to the diffractive gluon distribution. In the simplest case, the colorless exchange responsible for the rapidity gap is modeled by the exchange of two gluons (projected onto the color singlet state) coupled to the proton with some form factor or to a heavy onium which serves as a model of the proton [11, 12, 13].

We focus the following discussion on these dipole approaches of diffractive interactions (see Fig. 16). Then, the reaction follows three different phases displayed in Fig. 16 :

(1) the transition of the virtual photon to the $q\bar{q}$ pair (the colour dipole) at a large distance $l \sim \frac{1}{m_N x}$ of about 10-100 fm for HERA kinematics, upstream the target,

(2) the interaction of the color dipole with the target nucleon, and

(3) the projection of the scattered $q\bar{q}$ onto the diffractive system X.

The inclusive diffractive cross section is then described with three main contributions. The first one describes the diffractive production of a $q\bar{q}$ pair from a transversely polarized photon, the second one the production of a diffractive $q\bar{q}g$ system, and the third one the production of a $q\bar{q}$ component from a longitudinally polarized photon (see Fig. 16). In Fig. 17, we show that this two-gluon exchange model gives a good description of the diffractive cross section measurements [11, 12, 13].
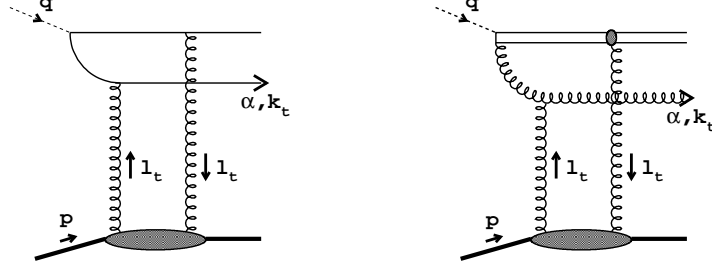
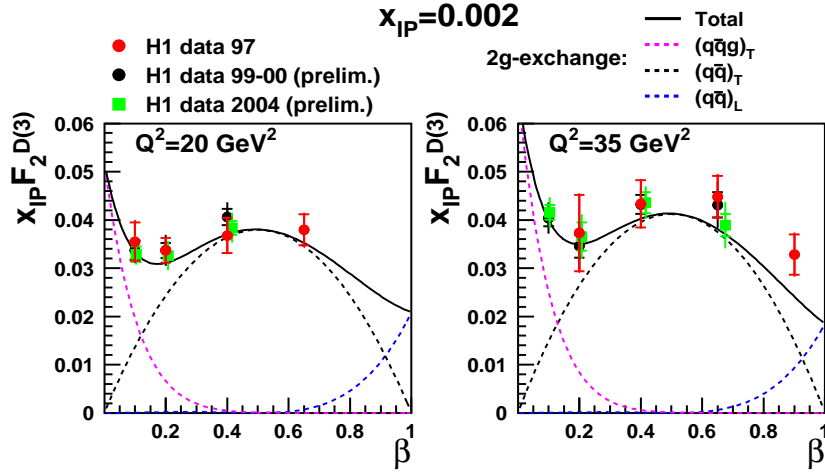Fig. 16. The $q\bar{q}$ and $q\bar{q}g$ components of the diffractive system.

Fig. 17. The diffractive structure function $x_{\mathbb{P}} F_2^{D(3)}$ is presented as a function of β for two values of Q^2. The different components of the two-gluon exchange model are displayed (see text). They add up to give a good description of the data. The structure function $x_{\mathbb{P}} F_2^{D(3)}$ is obtained directly from the measured diffractive cross section using the relation : $\frac{d^3 \sigma^{ep \to eXp}}{dx_{\mathbb{P}} \; dx \; dQ^2} \simeq \frac{4\pi \alpha_{em}^2}{xQ^4}(1 - y + \frac{y^2}{2}) F_2^{D(3)}(x_{\mathbb{P}}, x, Q^2)$, where y represents the inelasticity of the reaction.

One of the great advantage of the dipole approach is that it provides a natural explanation of the experimental observation that $\sigma^{diff}/\sigma^{tot} \simeq const$ as a function of energy W (see Fig. 6 and 7) [13]. Indeed, the dipole picture is valid in the frame in which the $q\bar{q}$ pair (dipole) carries most of the available rapidity $Y \sim \ln(1/x)$ of the system. The gluon radiation from the parent dipole can then be interpreted (in the large N_c limit) as a collection of
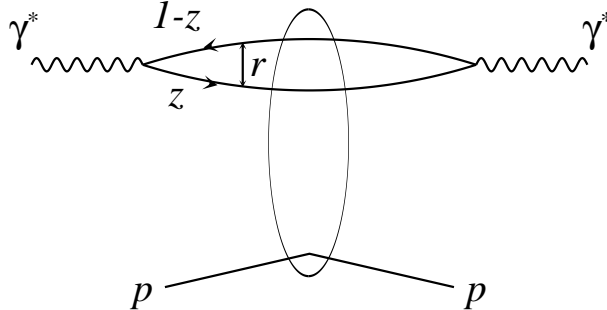
Fig. 18. Picture for the total cross section $(\gamma^* p \rightarrow \gamma^* p)$ in the dipole model.

dipoles of different transverse sizes which interact with the proton. If the proton stays intact, diffractive events with large rapidity gap are formed. In such case, the diffractive system is given by the color dipoles and the diffractive exchange can be modeled by color singlet gluons exchange (two-gluon exchange) between the dipole and the proton (see Fig. 18). When only the parent $q\bar{q}$ dipole forms a diffractive system, the diffractive cross section at $t = 0$ reads

$$\frac{d\,\sigma^{diff}}{dt}_{\mid t=0} = \frac{1}{16\,\pi} \int d^2 r\, dz\, |\Psi^\gamma(r,z,Q^2)|^2\ \hat{\sigma}^2(x,r), \qquad (1)$$

where Ψ^γ is the well known light-cone wave function of the virtual photon, r is the dipole transverse size and z is a fraction of the photon momentum carried by the quark. Applying the $q\bar{q}$ dipole picture to σ^{tot}, the following relation holds in the small-x limit

$$\sigma^{tot} = \int d^2 r\, dz\, |\Psi^\gamma(r,z,Q^2)|^2\ \hat{\sigma}(x,r), \qquad (2)$$

with the same dipole cross $\hat{\sigma}(x,r)$ as in Eq. (1). This Eq. (2) is pictured in Fig. 18.

The parameterization of $\hat{\sigma}(x,r)$ must be realized with caution [13, 12]. There are several features to consider. The density of gluons at given x increases with increasing Q^2, as described in perturbative QCD (see Fig. 19). According to QCD evolution it also increases at given Q^2 when x becomes smaller, so that the gluons become more and more densely packed. At some point, they will start to overlap and thus re-interact and screen each other. Then, we enter a regime where the density of partons saturates and where the linear QCD evolution equations cease to be valid. To quantify these effects, a saturation scale Q_s^2 can be introduced, which also depends on x, such that for $Q^2 \sim Q_s^2(x)$ these effects become important.
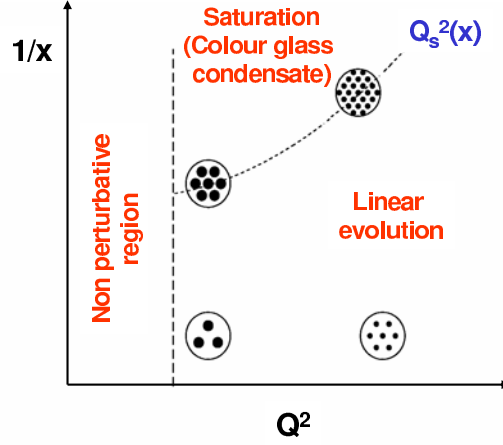
Fig. 19. Schematic view of the density of gluons in the transverse plane, as a function of the momentum fraction x and the resolution scale Q^2. Above the line given by $Q_s^2(x)$, saturation effects set in.
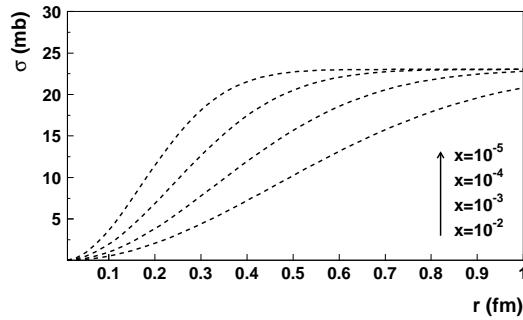

Fig. 20. The dipole cross section $\sigma_{q\bar{q}}$ in the saturation model as a function of dipole size r for different x (see text).

In practice, essential features of the saturation phenomenon are verified in the following parameterization for the dipole cross section proposed in Ref. [13]

$$\hat{\sigma}(x,r) = \sigma_0 \left\{ 1 - \exp(-r^2 Q_s^2(x)) \right\}, \qquad (3)$$

where $Q_s(x) = Q_0 \left(x/x_0 \right)^{-\lambda}$ is the saturation scale. In Fig. 20, we display the dipole cross section dependence of Eq. (3) as a function of r at given x in this model. At small dipole size $r \sim 1/Q$ (large Q^2), the cross section rises following the relation $\hat{\sigma}(x,r) \propto r^2 xg(x)$. At some value $R_s(x)$ of r,

the dipole cross section is so large that this relation ceases to be valid, and $\hat{\sigma}(x, r)$ starts to deviate from the quadratic behavior in r. Therefore, $R_s(x) = 1/Q_s(x)$ represents a typical saturation scale. As r continues to increase, $\hat{\sigma}(x, r)$ eventually saturates at a value typical of a meson-proton cross section. For smaller values of x, the initial growth of $\sigma_{q\bar{q}}$ with r is stronger because the gluon distribution is larger. The target is thus more opaque and saturation sets in at lower r.

Parameters of the dipole cross section of Eq. (3) are obtained from the analysis of inclusive data, and then can be used to predict diffractive cross sections in DIS. An important aspect of the form Eq. (3), in which r and x are combined into one dimensionless variable $rQ_s(x)$, is what is called geometric scaling, a new scaling property in inclusive DIS at small x. In Ref. [13], it has been shown to be valid for the total cross section.

It happens that diffraction in DIS is an ideal process to study parton saturation since this process is especially sensitive to the large dipole contribution, $r > 1/Q_s(x)$. Unlike inclusive DIS, the region below is suppressed by an additional power of $1/Q^2$. This makes diffractive interactions very important for tracting saturation effects. The dipole cross section with saturation (see Eq. (3)) leads in a natural way to the constant ratio (up to logarithms)

$$\frac{\sigma^{diff}}{\sigma^{tot}} \sim \frac{1}{\ln(Q^2/Q_s^2(x))} \, . \tag{4}$$

We can present very simply the main elements of the calculation that bring this result. Indeed, the photon wave function, in Eq. (1), favors small dipoles (small $r \sim 1/Q$), which gives

$$\frac{d\,\sigma^{diff}}{dt}_{\,|\,t=0} = \frac{1}{16\,\pi} \int d^2r \, dz \, |\Psi^\gamma(r, z, Q^2)|^2 \, \hat{\sigma}^2(x, r) \sim \frac{1}{Q^2} \int_{1/Q^2}^\infty \frac{dr^2}{r^4} \hat{\sigma}^2(x, r)$$

On the other hand, the dipole cross section favors relatively large dipoles, with $\hat{\sigma}(x, r) \sim r^2$. However, as discussed above in the building of Eq. (3), at sufficiently high energy, saturation cuts off the large dipoles already on the semi-hard scale $1/Q_s$. This leads to

$$\frac{d\,\sigma^{diff}}{dt}_{\,|\,t=0} \sim \frac{1}{Q^2} \int_{1/Q^2}^{1/Q_s^2} \frac{dr^2}{r^4}(r^2 Q_s^2)^2 \sim \frac{Q_s^2(x)}{Q^2} \propto x^{-\lambda} \tag{5}$$

and it follows immediately that $\frac{\sigma^{diff}}{\sigma^{tot}}$ is a constant of x at fixed values of Q^2. This result is illustrated experimentally in Fig. 6 and 7. We also present a fit of this model in Fig. 22 [6], using H1 and ZEUS inclusive diffractive data sets [3]. Parameters fitted in Fig. 22 are the ones discussed above σ_0,
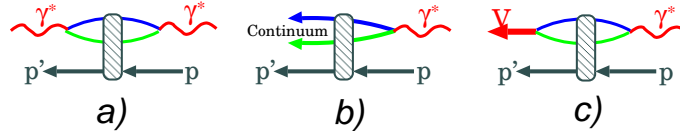
Fig. 21. The unified picture of Compton scattering, diffraction excitation of the photon into hadronic continuum states and into the diffractive vector meson

x_0 and λ [6]. A good description is found. A reasonable description is also obtained by keeping the original parameters as obtained in Ref. [13].

We have introduced above an interesting consequence of the dipole model for the total cross section: the geometric scaling property. Namely, the total cross section does not depend on x and Q^2 independently but can be expressed as a function of a single variable $\tau = Q^2/Q_s^2(x)$ [13]. This property has also been shown recently to be verified under minimal assumptions for all diffractive processes [14] (see Fig. 5). The experimental confirmation of this relation is an interesting piece of evidence that saturation effects are (already) visible in the inclusive diffractive DIS data. Extensions of these ideas at non-zero t values, rooted on fundamental grounds, have also been recently derived [12]. This provides essential perspectives to understand the transverse degrees of freedom which are discussed in the next sections.

Let us mention that one of the great interest of the two-gluon exchange approach is that it provides a unified description of different kind of processes measured in γ^*p collisions at HERA: inclusive $\gamma^*p \to X$, diffractive $\gamma^*p \to X\ p'$ and (diffractive) exclusive vector mesons (VM) production $\gamma^*p \to VM\ p'$ (see Fig. 21). In the last case, the step (3) described in the beginning of this section consists in the recombination of the scattered pair $q\bar{q}$ onto a real VM (as J/Ψ, ρ^0, ϕ,...) [15, 16, 17, 18] or onto a real photon for the reaction $\gamma^*p \to \gamma\ p'$. This process is called deeply virtual Compton scattering (DVCS) [19, 20].
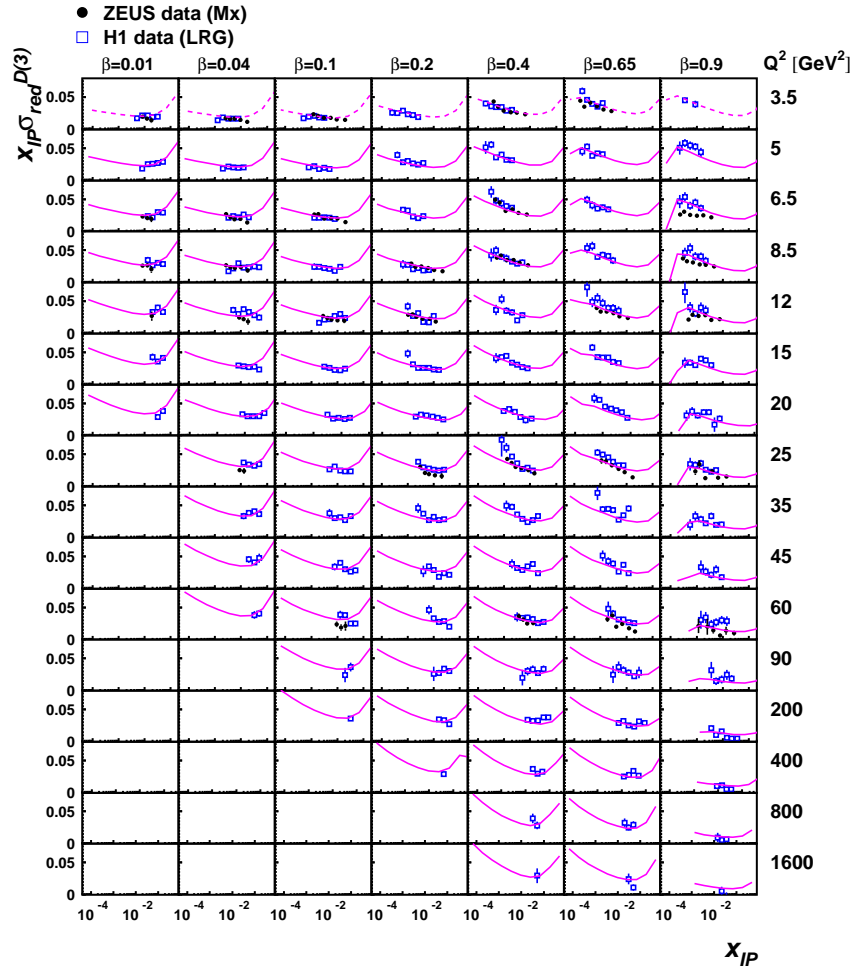
Fig. 22. Comparison of H1 and ZEUS inclusive diffractive data sets with the prediction of the dipole model of Ref. [13] (see Ref. [6]).
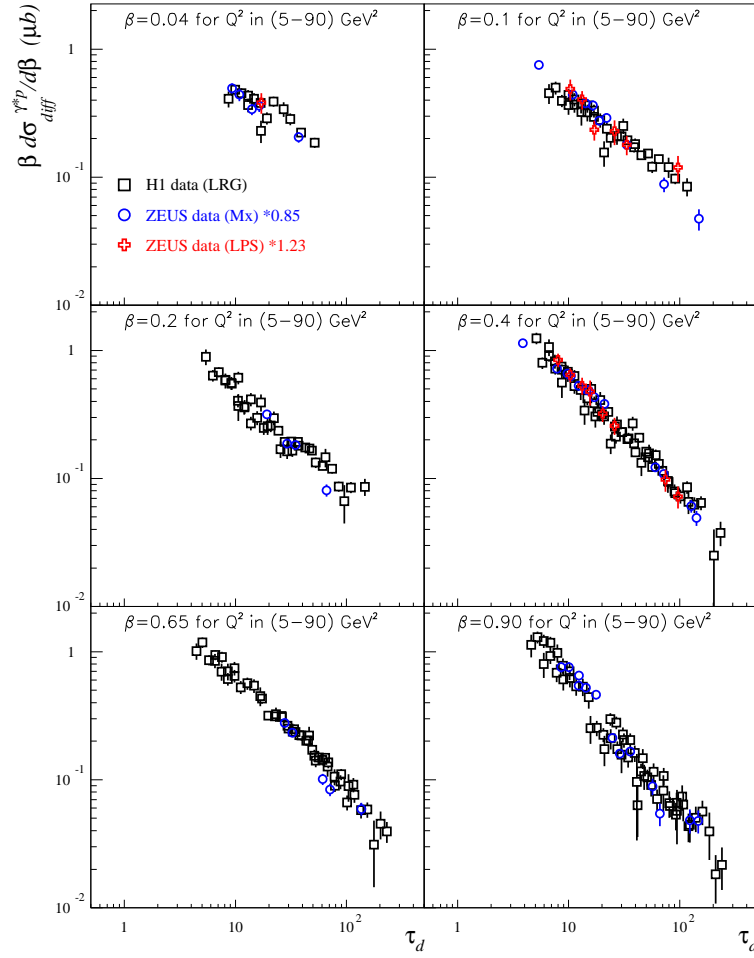
Fig. 23. The diffractive cross section $\beta \, d\sigma_{diff}^{\gamma^* p \to X p}/d\beta$ from H1 and ZEUS measurements, as a function of $\tau_d = Q^2/Q_s^2(x_{\mathbb{P}})$ in bins of β for Q^2 values in the range $[5;90]$ GeV^2 and for $x_{\mathbb{P}} < 0.01$ [14]. The geometric scaling is confirmed with a good precision.

6. Exclusive particle production

There is a long experimental and theoretical history to the study of vector meson production, revived with the advent of HERA. On the experimental side, the important result is that the cross sections for exclusive vector meson production rise strongly with energy when compared to fixed target experiments, if a hard scale is present. A compilation of experimental measurements are shown in Fig. 24 [15, 16, 17, 18]. For example, for J/ψ exclusive production, the mass of the J/ψ plays the role of the large scale.

Of course, this is not unexpected if we follow the discussion of the previous section, as VM cross sections, $\gamma^* p \to VM\ p'$, depend on the square of the gluon density in the proton. A first approximation of the cross section can then be written as

$$\left|\frac{d\sigma}{dt}\right|_{t=0}(\gamma^* N \to VN) = 4\pi^3 \Gamma_V m_V \alpha_s^2(Q)\frac{\eta_V^2\left(xg(x,Q^2)\right)^2}{3\alpha_{\text{em}}Q^6} \ , \qquad (6)$$

where the dependence on the meson structure is in the parameter

$$\eta_V = \frac{1}{2}\int \frac{dz}{z(1-z)}\phi^V(z)\left(\int dz\phi^V(z)\right)^{-1} \qquad (7)$$

and $\phi^V(z)$ is the leading-twist light-cone wave function.

The same behavior is observed for DVCS [19, 20], as shown in Fig. 25. Before discussing further the physics content of the W dependences, let us comment briefly the experimental result shown in Fig. 25. It displays DVCS cross section of nano-barn order. This is obviously an experimental challenge to measure cross sections at this small level of magnitude and this states also a difference between the low x_{Bj} kinematics and the case of fixed target experiments, that we discuss later. In fact, the DVCS process, $ep \to ep\gamma$, also receives a contribution from the purely electromagnetic Bethe-Heitler (BH) process, where the photon is emitted from the electron. The BH cross section is precisely calculable in QED and can be subtracted from the total process rate to extract the DVCS cross section. Of course, only if the BH contribution is not dominating the process rate. Otherwise, the subtraction procedure would be hopeless. It is the case at low x_{Bj}, and then for H1 and ZEUS experiments, the DVCS contribution can be measured directly. Fig. 26 presents the different contribution (for the scattered electron variables), after the experimental analysis of the reaction $ep \to ep\gamma$. We observe that DVCS and BH contributions are of similar size and thus, the BH contribution can be subtracted with a systematic uncertainty determined from a specific experimental study. In Fig. 27, we present the DVCS cross sections, $\gamma^* p \to \gamma p$, obtained over the full kinematic range of
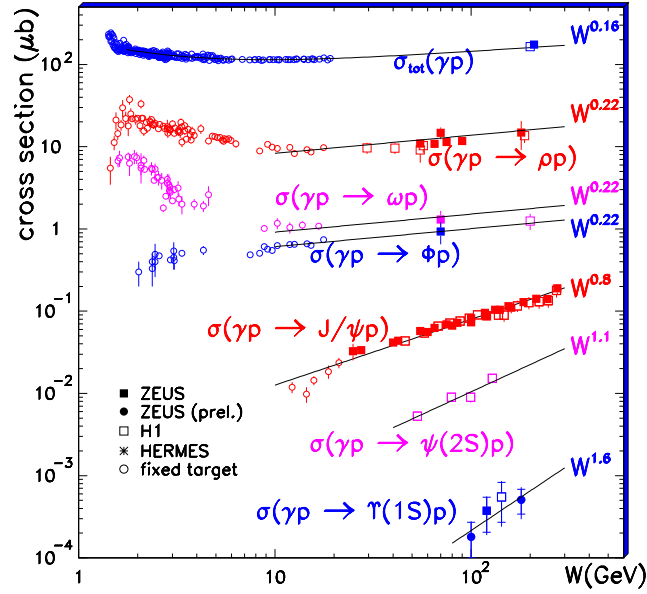
Fig. 24. W dependence of the exclusive vector meson cross section in photo-production, $\sigma(\gamma p \to Vp)$. The total photo-production cross section is also shown. The lines are the fit result of the form W^{δ} to the high energy part of the data.
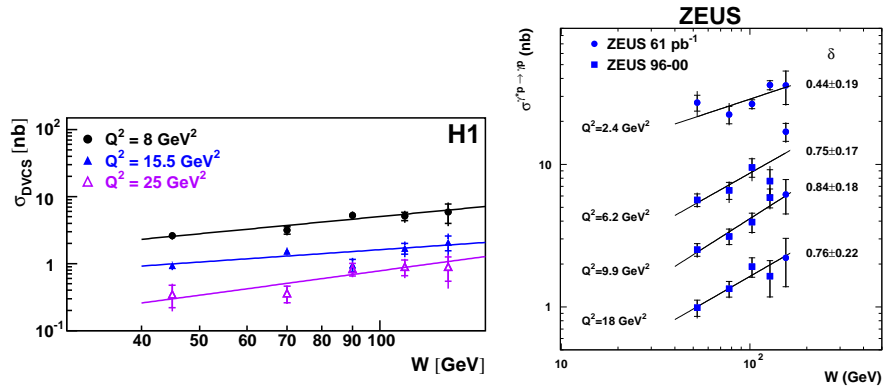

Fig. 25. The DVCS cross section, $\sigma^{\gamma^* p \to \gamma p}$, as a function of W for different Q^2 values. The solid lines are the results of a fit of the form $\sigma^{\gamma^* p \to \gamma p} \propto W^{\delta}$. The values of δ and their statistical uncertainties are given in the figure.

the analysis [19, 20], as a function of Q^2 and W. The behavior in W has been discussed qualitatively above, it corresponds to the dependence characteristic for a hard process. The Q^2 dependence, measured to be in $\sim 1/Q^3$ in Fig. 27, is also understandable qualitatively. Following the discussion of the previous section (see Eq. (5)), we expect a behavior of the imaginary DVCS amplitude ($\gamma^* p \to \gamma p$) in

$$ImA \sim \sigma_0 \frac{1}{Q^2} \int_{1/Q^2}^{1/Q_s^2} \frac{dr^2}{r^4}(r^2 Q_s^2) \tag{8}$$

which leads to a DVCS cross section of the form

$$\sigma \sim \sigma_0 (\frac{Q_s(x)^2}{Q^2})^2 \sim \frac{W^\delta}{Q^4}$$

With this expression, we find again the qualitative behaviour in W. Interestingly also, the measured Q^2 dependence in $\sim 1/Q^3$ is smaller than expected from this relation. In fact, to describe qualitatively the observed DVCS cross section, we must consider a parameterization in

$$\sigma \sim \sigma_0 \frac{W^\delta [Q^2]^\gamma}{Q^4},$$

after introducing a term in $[Q^2]^\gamma$ in the expression of the DVCS cross section. The term in $[Q^2]^\gamma$ is reminiscent from the QCD evolution of the DVCS amplitude (QCD evolution of the gluon distribution). The experimental observation in $\sigma \sim 1/Q^3$ is compatible with $\gamma \sim 1/2$ (using our notations). Of course, we do not stay at this qualitative understanding and we describe quantitative estimates of the DVCS cross sections in the following.

It is then clear that exclusive electro-production of light vector mesons [15, 16, 17, 18] and DVCS [19, 20] are particularly well suited processes to study the transition from the soft to the hard regime of strong interactions, using for example the scale Q^2 as a trigger. This transition can be observed experimentally in different ways when varying Q^2:

(1) In the change of the logarithmic derivative δ of the process cross section σ with respect to the $\gamma^* p$ center-of-mass energy W ($\sigma \sim W^\delta$). We expect a variation from a value of about 0.2 in the soft regime (low Q^2 values) to 0.8 in the hard one (large Q^2 values).

(2) In the decrease of the exponential slope b of the differential cross section with respect to the squared-four-momentum transfer t ($d\sigma/dt \sim e^{-b|t|}$), from a value of about 10 GeV^{-2} to an asymptotic value of about 5 GeV^{-2} when the virtuality Q^2 of the photon increases (see Fig. 34).
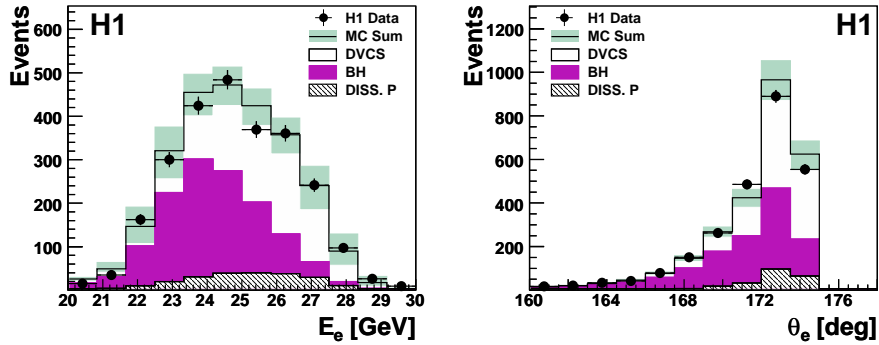
Fig. 26. Distributions of the energy and polar angle of the scattered electron. The data are compared with Monte Carlo expectations for elastic DVCS, elastic and inelastic BH and inelastic DVCS (labeled DISS. p). All Monte Carlo simulations are normalized according to the luminosity of the data. The open histogram shows the total prediction and the shaded band its estimated uncertainty.
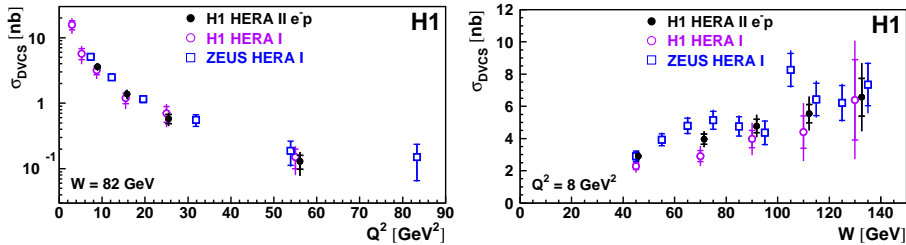

Fig. 27. The DVCS cross section as a function of Q^2 at $W = 82$ GeV and as a function of W at $Q^2 = 8$ GeV^2. The inner error bars represent the statistical errors, the outer error bars the statistical and systematic errors added in quadrature.

We illustrate this procedure on recent data on ρ^0 production [15]. The cross section $\sigma(\gamma^* p \to \rho^0 p)$ is presented in Fig. 28 as a function of W, for different values of Q^2. The cross section rises with W in all Q^2 bins. The same conclusion holds for DVCS, as shown in Fig. 25 [19, 20].

The soft to hard transition can also be seen by studying the W dependence of the cross section for exclusive vector meson photo-production, from the lightest one, ρ^0, to the heavier ones, up to the Υ, using this time
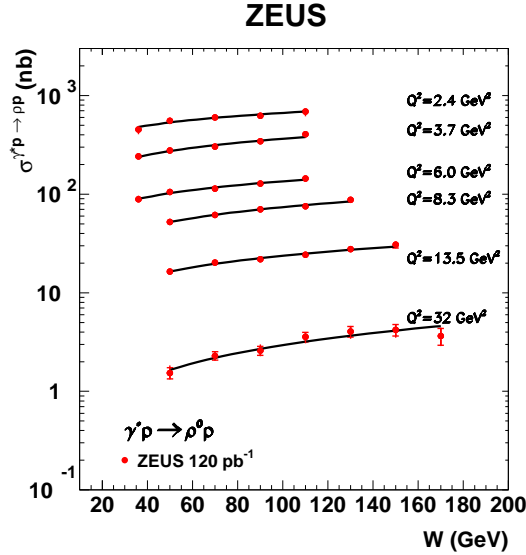
Fig. 28. W dependence of the cross section for exclusive ρ^0 electro-production, for different Q^2 values, as indicated in the figure. The lines are the fit results of the form W^δ to data.

the mass of the VM as the varying scale. Figure 24 shows $\sigma(\gamma p \rightarrow V p)$ as a function of W for light and heavy vector mesons. For comparison, the total photo-production cross section, $\sigma_{tot}(\gamma p)$, is also shown. The data at high W can be parameterized as W^δ, and the value of δ is displayed in the figure for each reaction. One sees clearly the transition from a shallow W dependence for low scales (soft) to a steeper one as the scale increases (hard) [15, 16, 17, 18].

A compilation of values of δ from DVCS and VM measurements are presented in Fig 29. Results are plotted as a function of $Q^2 + M^2$, where M is the mass of the vector meson (equal to zero in case of DVCS). We observe a universal behavior, showing an increase of δ as the scale becomes larger. The value of δ at low scale is the one expected from the soft Pomeron intercept, while the one at large scale is in accordance with twice the logarithmic derivative of the gluon density with respect to W.

A comment is in order concerning the W dependence of DVCS. It reaches the same value of δ as in the hard process of J/ψ electro-production. Given the fact that the final state photon is real, and thus transversely polarized, the DVCS process is produced by transversely polarized virtual photons, assuming s-channel helicity conservation. The steep energy dependence thus indicates that the large configurations of the virtual transverse photon are
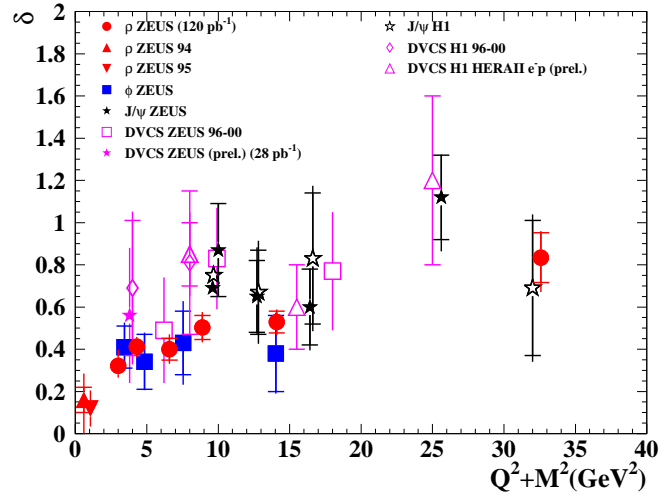
Fig. 29. A compilation of values of δ from fits of the form W^δ for exclusive VM electro-production, as a function of $Q^2 + M^2$. It includes also the DVCS results.
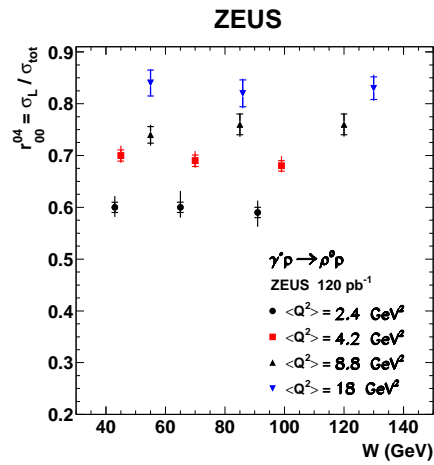
Fig. 30. The ratio $r^{04}_{00} = \sigma_L/\sigma_{tot}$ as a function of W for different values of Q^2.

suppressed and the reaction is dominated by small $q\bar{q}$ configurations (small dipoles), leading to the observed perturbative hard behavior. A similar effect is observed for ρ^0 production, as displayed in Fig. 30. The ratio σ_L/σ_{tot} is shown to be constant with W, which means that the W dependence for σ_L and σ_T are about the same [15].

Coming back to the discussion of the previous section on saturation, we can mention also that among diffractive interactions, exclusive vector meson production and DVCS are probably the best processes to study saturation effects in DIS since the transverse size of the $q\bar{q}$ pair forming a meson is controlled by the vector meson mass with $< r >= 1/\sqrt{M_V^2 + Q^2}$. Thus we expect saturation effects to be more important for larger (lighter) vector mesons. An interesting consequence of this feature is illustrated in Fig. 31 and 32, where we show that VM and DVCS process exhibit the property of geometric scaling [14]. In Fig. 32, we also demonstrate that this property of geometric scaling is verified at non-zero t values, within the present experimental uncertainty [12, 14]. In Fig. 32, we compare data with predictions of the dipole model, which essentially brings to a quantitative level the qualitative estimate given in Eq. (8) at the beginning of this section. We observe the very good agreement between data and predictions. This illustrates that this qualitative discussion (related to Eq. (8)) gives the main elements of understanding of the DVCS cross section dependences. More generally, as for all other diffractive processes presented in this review, it means that the mechanism included in the parameterization of the dipole cross section of the form written in Eq. (3) is correct and predictive. In practice, extensions of this formula are used in modern versions of the dipole model [12, 13], but with basically the same features.
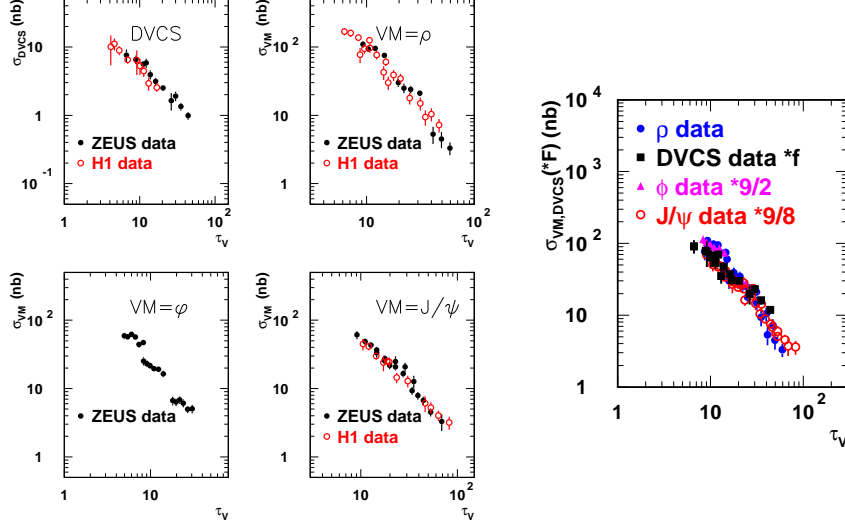
Fig. 31. Left: The ρ, J/Ψ and ϕ production cross-sections $\sigma_{VM}^{\gamma^*p\to Vp}$ and the DVCS cross-section $\sigma_{DVCS}^{\gamma^*p\to\gamma p}$ from H1 and ZEUS measurements, as a function of $\tau_V = (Q^2 + M_{VM}^2)/Q_s^2(x_{\mathbb{P}})$ and for $x_{\mathbb{P}} < 0.01$ [14]. Each process verifies the geometric scaling property. Right: We have rescaled cross sections by standard factors to compare all processes with the same definition of the abscissa scale τ_V (with $Q^2 > 5$ GeV^2). All processes verify the scaling property with the same definition of the scale.

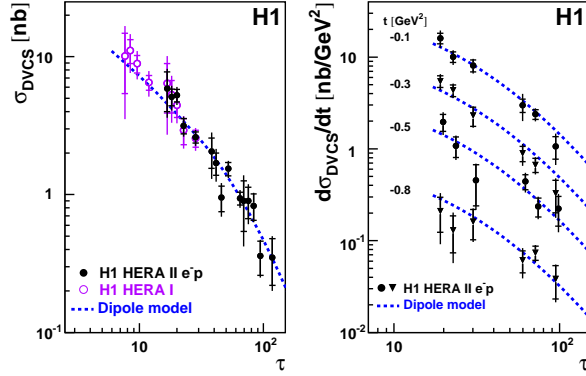Fig. 32. DVCS cross section measurements as a function of the scaling variable $\tau = Q^2/Q_s^2(x_{\mathbb{P}})$ for most recent data. The results are shown for the full t range $|t| < 1$ GeV^2 (left) and at four values of t (right). In both cases, the definition of the saturation scale is unchanged. Dipole model prediction [14], that naturally incorporates this effect, provides a good description of the data.

7. NUCLEON TOMOGRAPHY

We have briefly mentioned the decrease of the exponential slope b of the differential cross section with respect to t from a value of about 10 GeV^{-2} to an asymptotic value of about 5 GeV^{-2} when the virtuality Q^2 of the photon increases (see Fig. 34). With $t = (p - p')^2$ and $d\sigma/dt \sim e^{-b|t|}$. This is one of the key measurement in exclusive processes. In Fig. 33, we show that fits of the form $d\sigma/dt \sim e^{-b|t|}$ can describe DVCS measurements to a very good accuracy for different Q^2 and W values. The same conclusions hold in the case of VM production. That's the reason why we use this parameterization of the t dependence, with a factorized exponential slope b, to describe the HERA data on DVCS or VM production at low x_{Bj}.
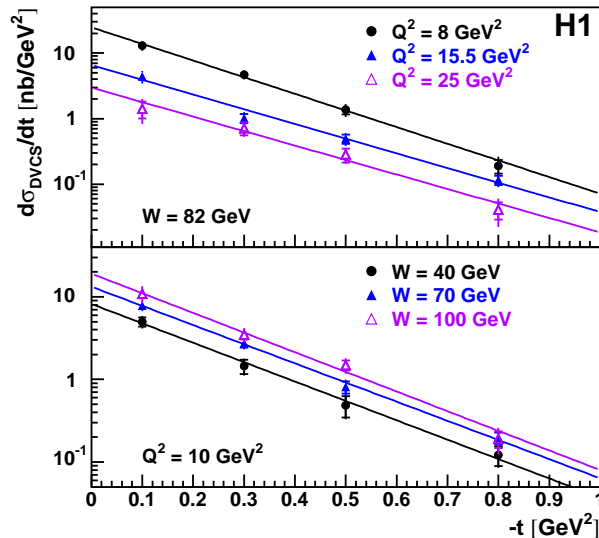
Fig. 33. The DVCS cross section, differential in t, for three values of Q^2 expressed atand for three values of W. The solid lines represent the results of fits of the form $e^{-b|t|}$.

The resulting values of b as a function of the scale $Q^2 + M^2$ are plotted in Fig. 34. A qualitative understanding of this behavior is simple. Indeed, b is essentially the sum of a component coming from the probe in $1/\sqrt{Q^2 + M_{VM}^2}$ and a component related to the target nucleon. Then, at large Q^2 or large M_{VM}^2, the b values decrease to the solely target component. That's why in Fig. 34, we observe that for large Q^2 or for the J/ψ, b is reaching a universal value of about 5 GeV^{-2}. This value is related to the size of the target probed during the interaction, as we show below, and we do not expect further decrease of b when increasing the scale, once a certain

scale is reached.

To understand this effect more quantitatively, we need to define a function that generalizes the gluon density which appears in Eq. (6) at non-zero t values. Then, we define a generalized gluon distribution F_g which depends on x and t (at given Q^2). From this function, we can compute a gluon density which also depends on a spatial degree of freedom, a transverse size (or impact parameter), labeled $R_\perp$, in the proton. Both functions are related by a Fourier transform

$$g(x, R_\perp; Q^2) \equiv \int \frac{d^2\Delta_\perp}{(2\pi)^2} e^{i(\Delta_\perp R_\perp)} F_g(x, t = -\Delta_\perp^2; Q^2).$$

At this level of the discussion, there is no need to enter into further details concerning these functions. We just need to know that the functions introduced above define proper (generalized) PDFs, with gauge invariance and all the good theoretical properties of PDFs in terms of operator product expansion. In fact, they are rooted on fundamental grounds [21], that we develop in further sections (without heavy formalism).

From the Fourier transform relation above, the average impact parameter (squared), $\langle r_T^2 \rangle$, of the distribution of gluons $g(x, R_\perp)$ is given by

$$\langle r_T^2 \rangle \equiv \frac{\int d^2 R_\perp \, g(x, R_\perp) \, R_\perp^2}{\int d^2 R_\perp \, g(x, R_\perp)} = 4 \frac{\partial}{\partial t} \left[\frac{F_g(x,t)}{F_g(x,0)} \right]_{t=0} = 2b, \qquad (9)$$

where b is the exponential t-slope. In this expression, $\sqrt{\langle r_T^2 \rangle}$ is the transverse distance between the struck parton and the center of momentum of the proton. The latter is the average transverse position of the partons in the proton with weights given by the parton momentum fractions. At low x_{Bj}, the transverse distance defined as $\sqrt{\langle r_T^2 \rangle}$ corresponds also to the relative transverse distance between the interacting parton (gluon in the equation above) and the spectator system, and therefore provides a natural estimate of the transverse extension of the gluons probed during the hard process. In other words, a Fourier transform of momentum to impact parameter space readily shows that the t-slope b is related to the typical transverse distance in the proton. This t-slope, b, corresponds exactly to the slope measured once the component of the probe itself contributing to b can be neglected, which means at high scale: Q^2 or M_{VM}^2. Indeed, at high scale, the $q\bar{q}$ dipole is almost point-like, and the t dependence of the cross section is given by the transverse extension of the gluons in the proton for a given x_{Bj} range.

A short comment is in order concerning the fundamental relation (9) for DVCS at HERA (at low x_{Bj}). Does it make sense to keep only the gluon distribution in this expression or do we need to consider also sea quarks?

This issue can be addressed simply by coming back to Eq. (8), where we have approximated the imaginary DVCS amplitude ($\gamma^* p \to \gamma p$) in

$$ImA \sim \sigma_0 \frac{1}{Q^2} \int_{1/Q^2}^{1/Q_s^2} \frac{dr^2}{r^4} (r^2 Q_s^2).$$

Let us give first a more general form to this formula, keeping the tracks of the photon wave functions

$$ImA = \int d^2 r \, dz \, \Psi^*(r, z, Q_1^2 = Q^2) \Psi(r, z, Q_2^2 = 0) \hat{\sigma}(x, r), \qquad (10)$$

where $\Psi^*(r, z, Q_1^2 = Q^2)$ is the wave function for the virtual photon and $\Psi(r, z, Q_2^2 = 0)$ for the real photon. Also, following the previous discussion on the dipole cross section, we can write: $\hat{\sigma}(x, r) \sim \sigma_0 r^2 Q_s(x, r)^2$, with

$$Q_s(x, r)^2 \sim \frac{\alpha_S \, xg(x, 1/r^2)}{\pi R_p^2} \sim Q_0^2 (\frac{x_0}{x})^\lambda,$$

where R_p is the proton radius. We conclude immediately that the imaginary part of the DVCS amplitude is dependent on the gluon density convoluted by the photon (virtual and real) wave functions. It gives the rationale behind formula (9). Of course, this is a matter of representation. In the Eq. (10), we write the photon-gluon interaction through a quark loop, with a virtual photon fluctuating in a $q\bar{q}$ pair, which is exactly the dipole $q\bar{q}$ component entering in $\Psi^*(r, z, Q_1^2 = Q^2)$ (see also Fig. 21). In other words, at low x_{Bj} ($x_{Bj} \simeq 10^{-3}$), the idea is that quarks (sea quarks) are produced by gluons and the dipole formalism, summarized in Eq. (10) or Fig. 21, provides a very powerful expression of this behavior. Of course, in other formalisms, that we present latter, we can express the cross sections at the level of the photon-quark interaction and thus consider directly the sea quark distribution.

DVCS results lead to $\sqrt{r_T^2} = 0.65 \pm 0.02$ fm at large scale $Q^2 > 8$ GeV^2 for $x_{Bj} \simeq 10^{-3}$ [19]. This value is smaller than the size of a single proton, and, in contrast to hadron-hadron scattering, it does not expand as energy W increases (see Fig. 35). Then, we can parametrize the measured b values displayed in Fig. 35 in the form of a Pomeron trajectory: $b = b_0 + 2\alpha' \ln \frac{1}{x_{Bj}}$. We obtain that the α' value, which is characteristic of the energy dependence of the trajectory, is close to zero. It is not useless to recall that is is extremely challenging on the experimental analysis side. We are dealing with nano-barn cross sections, that we measure as a function of t, and finally, we measure the energy dependence of this behavior in t. Of course,
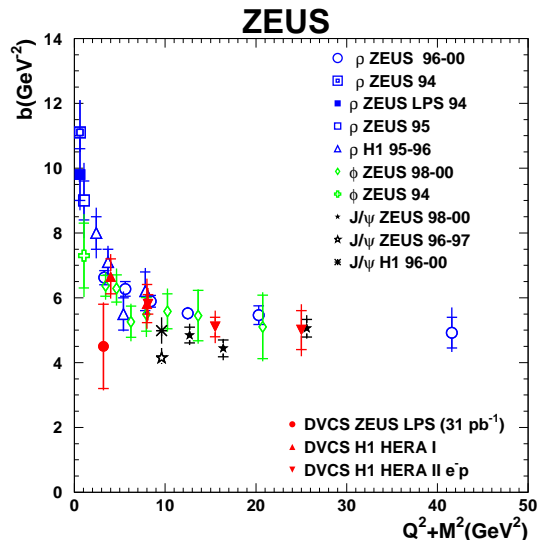
Fig. 34. A compilation of the values of the slope b as a function of $Q^2 + M^2$ for various exclusive processes including the present DVCS measurement. The inner error bars represent the statistical uncertainty while the outer error bars the statistical and systematic uncertainties added in quadrature. Note that the latest t slope measurement of DVCS by the ZEUS collaboration [20] is shown. It falls below (1 sigma effect) the H1 measurement at a comparable Q^2 value [19]. The main result does not change: at large Q^2, exponential t slopes converge to a scaling value (see text) ans this is a common trend for all VM processes. However, at low Q^2 ($Q^2 \simeq 3$ GeV^2), ZEUS result indicates the absence of effects in $b \sim 1/Q^2$ (from the probe) for DVCS, whereas H1 result shows a behavior comparable to ρ at this Q^2, with a clear influence of the probe to the building of the measured b.

the gain is important. In particular, the great interest of the DVCS is that the t dependence measured is free of effects that could come from VM wave functions (in case of VMs) and then spoil (to a certain limit) the interpretation of b described above. With DVCS, we have thus the advantage to work in a controlled environment (photon wave functions) where the generic Eq. (9) can be applied to the measurement (almost directly) and must not be corrected with effects arising from VMs wave function.

It is obviously very interesting to extend the result presented in Fig. 35 to all VMs. Indeed, we can study the W dependence of $d\sigma/dt$ and extract the energy dependence as done above for all VMs, using $b = b_0 + 2\alpha' \ln \frac{1}{x_{Bj}}$. Results are presented in Fig. 36 (bottom). Values are plotted as a function of $Q^2 + M^2$. We observe that the values of α' tends to decrease with the
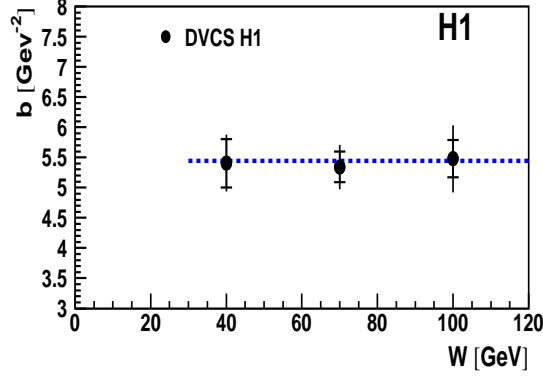
Fig. 35. The logarithmic slope of the t dependence for DVCS as a function of W.
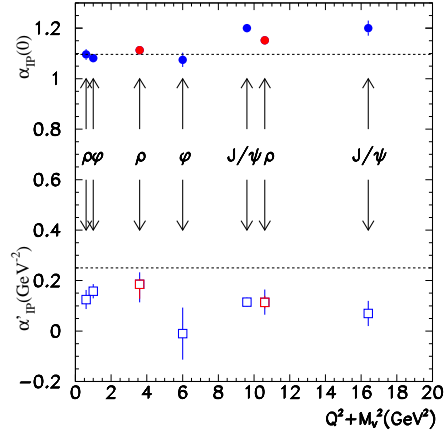
Fig. 36. Values of the intercept and slope of the effective Pomeron trajectory as a function of $Q^2 + M^2$, as obtained from measurements of exclusive VM electro-production.

scale. In particular, the measurement of α' done for the J/Ψ [17], leading to a small value for α', is well compatible with the DVCS result [19]. A short comment can be done qualitatively on such small α' value. We can rephrase this observation as an evidence of no shrinkage of $d\sigma/dt$ in the process $\gamma^*p \to J/\Psi p$ or $\gamma^*p \to \gamma p$. Looking at the diagram describing two gluon exchange in Fig. 37, the virtual photon fluctuates into two high k_T quarks. Although in the diagram there are only two gluons linked to the proton, we actually have a whole ladder due to the large rapidity range available at these

Fig. 37. A diagram describing a gluon ladder in a diffractive process.

high W energies (see Fig. 37). From the virtual photon vertex down to the proton, the average k_T of the gluons gets smaller, the configuration larger and we enter the region of low k_T physi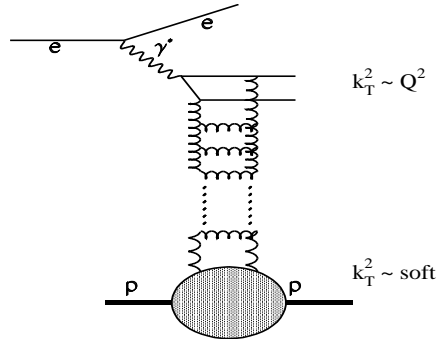cs governed by non-perturbative QCD. This process is called Gribov diffusion. Thus a process can start as a hard process at the photon vertex but once it couples to the proton it gets a soft component which makes the process non calculable in pQCD. The average k_T of the partons in the process can be estimated by the slope of the trajectory since $\alpha' \sim 1/ < k_T >$. The fact that no shrinkage is observed indicates that Gribov diffusion is not important in this process at the presently available W values, and the average k_T remains large. Such a behavior is expected for hard processes, where $\alpha' \ll 0.25$ GeV^{-2}. The experimental results for exclusive J/Ψ production and DVCS confirm that both processes are fully calculable in perturbative QCD.

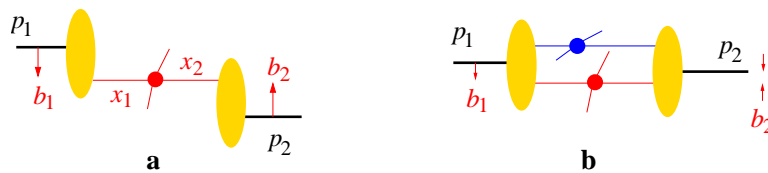Fig. 38. a: Graph with a single hard interaction in a hadron-hadron collision. The impact parameters b_1 and b_2 are integrated over independently. b: Graph with a primary and a secondary interaction.

Let us finish this section by a comment making the link with LHC issues. Indeed, the correlation between the transverse distribution of partons and their momentum fraction is not only interesting from the perspective

of hadron structure, but also has practical consequences for high-energy hadron-hadron collisions. Consider the production of a high-mass system (a dijet or a heavy particle). For the inclusive production cross section, the distribution of the colliding partons in impact parameter is not important: only the parton distributions integrated over impact parameters are relevant according to standard hard-scattering factorization (see Fig. 38(a)). There can however be additional interactions in the same collision, especially at the high energies for the Tevatron or the LHC, as shown in Fig. 38(b). Their effects cancel in sufficiently inclusive observables, but it does affect the event characteristics and can hence be quite relevant in practice. In this case, the impact parameter distribution of partons must be considered. The production of a heavy system requires large momentum fractions for the colliding partons. A narrow impact parameter distribution for these partons forces the collision to be more central, which in turn increases the probability for multiple parton collisions in the event (multiple interactions).

8. Generalised parton distributions

We have already defined in the previous section a first form for a generalized gluon distribution. In this part, we move into further details and explain the wide experimental field opened in the area of generalized parton distributions. First, a short contrarian comment: DIS can not be considered as the continuation of the original Rutherford experiment. Indeed, Rutherford measured that the nucleus is concentrated in a very small part of the atom, and, as far as we consider only PDFs, we have no possibility to explore the spatial structure of the nucleon. The reason is that in the infinite momentum frame picture, the light-cone description of the Feynman parton model does not explore the space-time location of partons. In other words, within the infinite momentum frame description, the variable x_{Bj} has no direct relation to the space coordinate of a parton but is related to a combination of the energy and momentum of this parton.

In the previous section, we have shown that data on exclusive particle production can give access to the spatial distribution of quarks and gluons in the proton at femto-meter scale. Then, we have defined functions, which model this property (for gluons) through the relation

$$g(x, R_\perp; Q^2) \equiv \int \frac{d^2\Delta_\perp}{(2\pi)^2} e^{i(\Delta_\perp R_\perp)} F_g(x, t = -\Delta_\perp^2; Q^2).$$

Of course, a similar relation holds for quarks, linking the two functions $q(x, R_\perp; Q^2)$ and $F_q(x, t = -\Delta_\perp^2; Q^2)$. The general framework for this physics is encoded in the generalized parton distributions (GPDs). We

already know that the reconstruction of spatial images from scattering experiments by way of Fourier transform of the observed scattering pattern is a technique widely used in physics, for example in X-rays scattering from crystals. In simple words, what we have done experimentally is that we have extended this technique to the spatial distribution of quarks and gluons within the proton, using processes that probe the proton at a tiny resolution scale. Of course, as already mentioned, working at a femto-meter scale with nano-barn cross sections is very challenging from the experimental front. We have achieved this and it immediately opens a way in the ambitious program of mapping out the GPDs. We come back below in a more systematic way on different aspects of that program that requires a large amount of experimental informations, for which future programs at JLab and CERN are appealing.
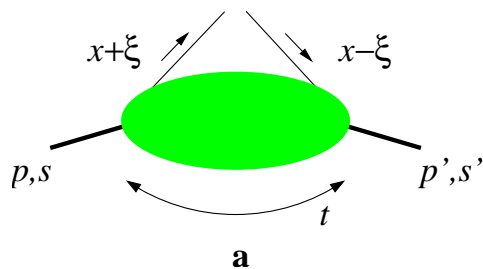
a

Fig. 39. Picture of a GPD and its variables. The momentum fractions x and ξ refer to the average hadron momentum $\frac{1}{2}(p + p')$. Note that x is an internal variable and is not equal to x_{Bj}. However, there is a relation between the skewing variable ξ and x_{Bj}, $\xi = x_{Bj}/(2 - x_{Bj})$.

Before coming back to the experimental side, we can present a short overview of GPDs, in simple terms. It is interesting, even for an experimentalist, as it clarifies the Fourier transform relation discussed above and makes more transparent the goals for the future. For complete reviews, see Ref. [21, 22, 23]. GPDs are defined through matrix elements $\langle p'|\mathcal{O}|p\rangle$ between hadron states $|p'\rangle$ and $|p\rangle$, with non-local operators $\mathcal{O}$ constructed from quark and gluon fields. From this expression, we understand why GPDs are directly related to the amplitude for VM or real gamma exclusive production. For unpolarized quarks there are two distributions $H^q(x, \xi, t)$ and $E^q(x, \xi, t)$, where x and ξ are defined in Fig. 39. The former is diagonal in the proton helicity, whereas the latter describes proton helicity flip. For $p = p'$ and equal proton helicities, we recover the diagonal matrix element parameterized by usual quark and antiquark densities, so that $H^q(x, 0, 0) = q(x)$ and $H^q(-x, 0, 0) = -\bar{q}(x)$ for $x > 0$. Note that the

functions of type E are not accessible in standard DIS, as it corresponds to matrix elements $\langle p', s'|\mathcal{O}|p, s\rangle$ with $s \neq s'$. Even in DVCS-like analysis, it is very difficult to get a sensitivity to these functions, as in most observables, their contributions are damped by kinematic factors of orders $|t|/M_p^2$, with an average $|t|$ value in general much smaller that 1 GeV^2. Then, till stated otherwise, our next experimental discussions are concentrated on the determination of GPDs H_q and H_g. We come back later on this point and show specific cases where E-type functions can be accessed and why this is an important perspective. An interesting property of GPDs, which lightens their physics content, is that their lowest moments give the well-known Dirac and Pauli form factors

$$\sum_q e_q \int dx\, H^q(x, \xi, t) = F_1(t) \qquad \sum_q e_q \int dx\, E^q(x, \xi, t) = F_2(t),$$

(11)

where e_q denotes the fractional quark charge. It means that GPDs measure the contribution of quarks/gluons with longitudinal momentum fraction x to the corresponding form factor. In other words, GPDs are like mini-form factors that filter out quark with a longitudinal momentum fraction x in the proton. Therefore, in the same way as Fourier transform of a form factor gives the charge distribution in position space, Fourier transform of GPDs (with respect to variable t) contains information about the spatial distribution of partons in the proton. This discussion clarifies also the Fourier transforms linking $g(x, R_\perp; Q^2)$ and $F_g(x, t = -\Delta_\perp^2; Q^2)$ or $q(x, R_\perp; Q^2)$ and $F_q(x, t = -\Delta_\perp^2; Q^2)$. From these relations, it follows that $q(x, R_\perp; Q^2)$ is the probability density to find a quark with momentum fraction x at a transverse distance $R_\perp$ from the (transverse) center of momentum of the proton. More formal discussions can be found in Ref. [21]. More exactly, what must be confronted with the proton radius is not $\sqrt{r_T^2}$ but $\sqrt{r_T^2/(1 - x_{Bj})}$, which does not change our result with $x_{Bj} \simeq 10^{-3}$ ($\sqrt{r_T^2} = 0.65 \pm 0.02$ fm), but must be taken into account for fixed target kinematics at larger x_{Bj}. In particular, at very large x_{Bj} ($x_{Bj} \to 1$), the struck quark is carrying almost the entire proton momentum, thus its relative distance to the center of momentum of the proton obviously tends to zero. This means that $\sqrt{r_T^2}$ tends to zero (by definition). In order to keep finite the ratio $\sqrt{r_T^2/(1 - x_{Bj})}$, we can conclude that the asymptotic form of $\sqrt{r_T^2}$ at large x_{Bj} is in $(1 - x_{Bj})^2$.

More exactly, the distance $\sqrt{r_T^2/(1 - x_{Bj})}$ is the associated transverse distance between the struck parton (probed during the hard interaction) and the center of momentum of the spectators. That's why it can be interpreted

as a typical spatial extension of partons in the proton. What we have learned so far with the present experimental situation is already very rich: slow partons (at low x_{Bj}) are located at the periphery of the proton whereas fast partons (at large x_{Bj}) make up the core of the proton (in its center). This last property is only an indirect observation from fits of form factor measurements [22] (see below for a short discussion).

We need to get more information. How large can be the spread in space of slow partons? Could it be larger that 1 fm? Also, what is the spread for the large x (constituent) partons? Where is the transition between the large x partons and the peripheric partons? We need more experimental results and then more experiments with different setups to address these questions from all possible angles.

For example if we would observe a gradual increase of the t dependence of the GPD $H(x, 0, t)$ (quarks or gluons) when varying x_{Bj} from large to small values, it would mean exactly that quarks at large x_{Bj} come from the more localized valence core of the proton, while the small x_{Bj} region receives contribution from the periphery or, in other words, from the wider meson cloud. This is a very nice perspective for the future to expect direct measurements of $\sqrt{r_T^2}$ from many experiments in the world.

Let us come back briefly to form factors and their essential role in the interplay between x and t kinematic variables. A complete analysis is presented by Diehl et al. in Ref. [24]. Indeed, it is clear that indirect information on impact parameter distributions can be obtained by using the sum rules presented in Eq. (11), which provides a natural link between the GPDs dependences in x and t. We can exemplify the structure of the link on the Dirac form factor for proton and neutron

$$F_1^p(t) = \int_0^1 dx [\frac{2}{3} H_v^u(x,t) - \frac{1}{3} H_v^d(x,t)]$$

$$F_1^n(t) = \int_0^1 dx [\frac{2}{3} H_v^d(x,t) - \frac{1}{3} H_v^u(x,t)]$$

where we have neglected the contribution from the s quarks. Note that only valence type distributions appear in these relations, since the electromagnetic current is only sensitive to the difference of quark and antiquark distributions. Then, from an ansatz for the functional dependence of $H_v^q(x, 0, t)$ and measurements of the Dirac form factor $F_1(t)$, a fit of some GPDs parameters can be performed [24]. Obviously, the sensitivity of such a fit is governed by the parameters building the interplay of x and t dependences (for valence distributions), which is the purpose of this approach.

9. QUANTIFYING SKEWING EFFECTS ON DVCS AT LOW x_{Bj}

After this short overview of GPDs physics, we understand clearly why DVCS is the typical (and cleanest) process to extract GPDs, or at least to extract informations on GPDs. Then, we come back on the DVCS cross section measurements and their interpretation in terms of GPDs. In order to quantify the magnitude of skewing effects, and thus the impact of GPDs on the DVCS process ($\gamma^* p \rightarrow \gamma p$), we need to derive for example the following ratio from measured cross sections [19]

$$R \equiv Im\, A\, (\gamma^* p \rightarrow \gamma p)_{t=0}/Im\, A\, (\gamma^* p \rightarrow \gamma^* p)_{t=0}.$$

In this expression, $ImA(\gamma^* p \rightarrow \gamma p)_{t=0}(Q^2, W)$ is the imaginary part of the DVCS process and is directly proportional to the GPDs [22]. Also, the term $Im\, A\, (\gamma^* p \rightarrow \gamma^* p)_{t=0}$ is directly proportional to the total cross section. The ratio R is then is equivalent to the ratio of the GPDs to the PDFs. That's why its measurement can provide directly the impact of GPDs, when compared to pure PDFs predictions. In Ref. [25], we have shown how to extract this ratio from the DVCS and DIS cross sections. Results are presented in Fig. 40. The typical values of R are found around 2 [22], whereas in a model without skewing R would be equal to unity. Therefore, the present measurements confirm the large effect of skewing.

Values of R are also compared with a GPDs model based on a forward ansatz at low scale ($Q_0 = 1.3$ GeV). Namely, the singlet GPD is parametrized as follows: $H_S(x, \xi) = Q_S(x)$, where $Q_S(x)$ is the singlet PDFs and x and ξ are the variables used in the previous part for the definition of GPDs (see Fig. 39). It does not mean that the GPD is taken to be exactly the PDF. Indeed, at $x = \xi$, we get $H_S(\xi, \xi) = Q_S(\xi) = Q_S(x_{Bj}/2)$ and not $Q_S(x_{Bj})$. In other words, in this forward ansatz parameterization of the GPDs, we simply consider that at a low scale Q_0, we can forget the profile function and take directly the parameterization of the GPD from a PDF like form. The same is done with non-singlet and gluon distributions. If the GPDs are parametrized in such a way at initial scale, then we have two possibilities. Either, we evolve the GPDs using skewed QCD evolution equations, which naturally generates the skewing dependence (in ξ) along the Q^2 evolution, or we forget about the skewed evolution and we consider only the standard QCD evolution equations like for PDFs. This corresponds to the two curves presented in Fig. 40. The full line represents the complete GPDs model, with skewed evolution equations and the dashed curve, labeled forward ansatz (all Q^2), represents the case where initial distributions are evolved with standard QCD evolution equations. Then, Fig. 40 demonstrates that we need the full GPDs model to describe our data on DVCS cross sections (converted in R values). If we forget about the skewing
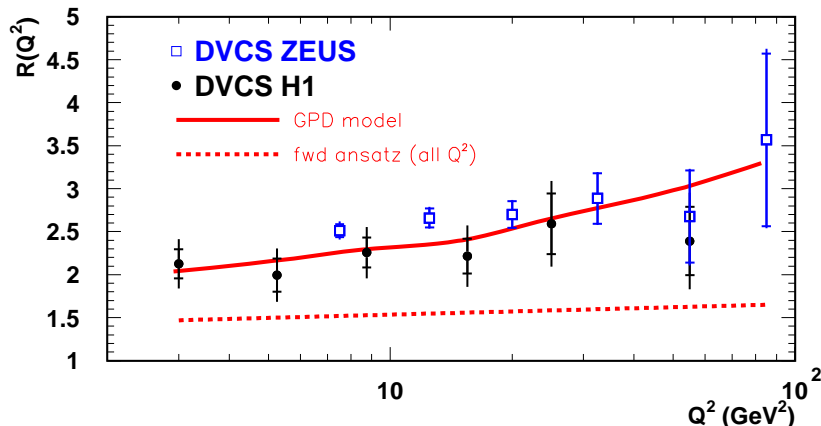
Fig. 40. Skewing factor $R \equiv \mathcal{I}m\, A\,(\gamma^* p \rightarrow \gamma p)_{t=0}/\mathcal{I}m\, A\,(\gamma^* p \rightarrow \gamma^* p)_{t=0}$ extracted from DVCS and DIS cross sections [25] The GPD model is also displayed and gives a good agreement of the data (full line). The forward ansatz model, used at all values of Q^2, fails to reproduce the total skewing effects generated by the QCD evolution (dashed line).

generated during the QCD evolution, we miss the data by about 30%. This is clearly a deep impact of the skewing effects present in the data.

Another influence of GPDs that we can check on data concerns the t dependence. We have already shown that in the kinematic domain of H1 and ZEUS measurements, DVCS cross section $(d\sigma/dt)$ can be factorized and approximated to a good accuracy by an exponential form $e^{-b|t|}$, which implies a factorized dependence in $e^{-b/2|t|}$ for GPDs. However, we can think of taking into account a non-factorized form in $|x|^{-\alpha'/2t}$ as well. With the small α' value determined previously, we know that this term can only be small (negligible) correction to the dominant (factorized) t dependence in $e^{-b/2|t|}$ for GPDs.

10. On the way of mapping out the GPDs

As we have seen, the mapping of the GPDs is certainly a difficult work due to the flexibility of these functions. However, we have already illustrated some elements that can be constrained with the present DVCS data at low x_{Bj}. Concerning the t dependence of the GPDs in this kinematic domain, we have shown that the impact of a potential non-factorized term in $|x|^{-\alpha't}$ is small, due to the small value of α' observed at low x_{Bj}. This is one important

element of the experimental project to measure DVCS at COMPASS in the future,as we need to check this kind of effects at larger x_{Bj}. DVCS at COMPASS (located at CERN) can be measured with muon beams on fixed target, $\mu p \to \mu p \gamma$. If the muon energy is large enough, for example $E_\mu = 190$ GeV, DVCS dominates over the BH contribution (as for H1 and ZEUS) so that DVCS cross section can be measured directly. At smaller lepton energy, $E_\mu = 100$ GeV, the interference between BH and DVCS becomes large and offers the opportunity to study interference between both processes. The strong interest is that the x_{Bj} kinematic domain of COMPASS follows the one of H1 and ZEUS at larger x, with $x_{Bj} \sim [0.05 - 0.15]$, thus much larger values than in the kinematic domain of H1 and ZEUS. A project is ongoing to install a proton recoil detector after 2010 and then measure DVCS cross sections [28]. Some tests have already been done to show the technical feasibility of the proposed experiment.

Let us discuss how we can access an interference between DVCS and BH reactions. In fact, since these two processes have an identical final state, they can obviously interfere. The squared photon production amplitude is then given by

$$|A|^2 = |A_{BH}|^2 + |A_{DVCS}|^2 + \underbrace{A_{DVCS}\,A_{BH}^* + A_{DVCS}^*\,A_{BH}}_{I}, \qquad (12)$$

where A_{BH} is the BH amplitude, A_{DVCS} represents the DVCS amplitude and I denotes the interference term. For unpolarized proton target and lepton beam, the interference term can be written quite generally as a linear combination of harmonics of the azimuthal angle ϕ, which is the angle between the plane containing the incoming and outgoing leptons and the plane defined by the virtual and real photons. In the leading twist approximation, if only the first term in $\cos\phi$ and $\sin\phi$ are considered, it can be written as: $I \propto -C\,[a\cos\phi\,\mathrm{Re}A_{DVCS} + bP_l\sin\phi\,\mathrm{Im}A_{DVCS}]$. In this expression, $C = \pm 1$ is the lepton beam charge, P_l its longitudinal polarization and a and b are functions of the ratio of longitudinal to transverse virtual photon flux [22]. At COMPASS, if we measure a beam charge asymmetry (BCA), the polarization of the muon beam flips with the charge and so, the $\sin\phi$ terms disappears. Then, the BCA reads

$$A_C = \frac{d\sigma^+/d\phi - d\sigma^-/d\phi}{d\sigma^+/d\phi + d\sigma^-/d\phi} \sim p_1\cos\phi = 2A_{BH}\frac{\mathrm{Re}A_{DVCS}}{|A_{DVCS}|^2 + |A_{BH}|^2}\cos\phi. \tag{13}$$

Note that DVCS cross section measurements which are integrated over ϕ are not sensitive to the interference term. Simulations done for COMPASS [28] are shown in Fig. 41 for BCA in a setup described in the legend of the figure. Two models of GPDs, with a factorized and non-factorized t

dependence, are shown in Fig. 41 and we can observe easily the great discrimination power offered by COMPASS, with the proton recoil detector fully operational [28]. Of course, the discrimination is large in Fig. 41 due to the fact that α' is taken to be large ($\alpha' \sim 0.8$ GeV^{-2}) in simulations. If it happens to be much smaller, as measured at low x_{Bj} by H1 [19] (see previous section), both predictions for BCA in Fig. 41 would be of similar shape, as both curves would converge to the factorized case.
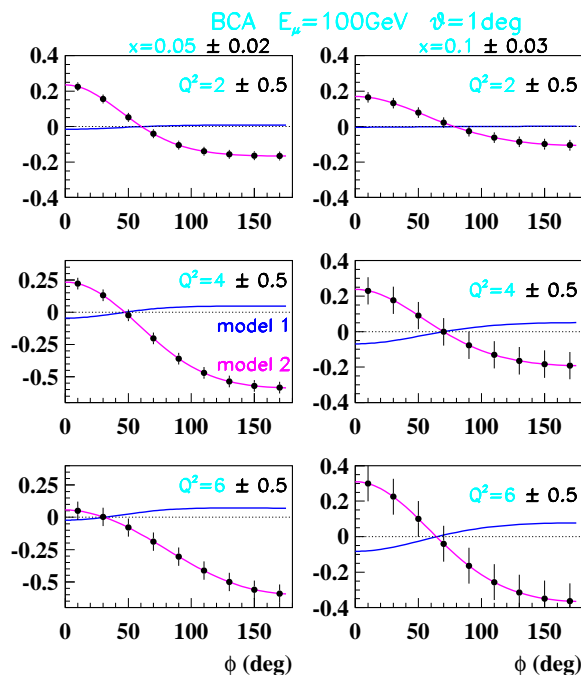

Fig. 41. Azimuthal distribution of the beam charge asymmetry measured at COMPASS at $E_\mu = 100$ GeV and $|t| \leq 0.6$ GeV^2 for 2 domains of x_{Bj} ($x_{Bj} = 0.05 \pm 0.02$ and $x_{Bj} = 0.10 \pm 0.03$) and 3 domains of Q^2 ($Q^2 = 2 \pm 0.5$ GeV^2, $Q^2 = 4 \pm 0.5$ GeV^2 and $Q^2 = 6 \pm 0.5$ GeV^2) obtained in 6 months of data taking with a global efficiency of 25% and with $2 \cdot 10^8$ μ per SPS spill ($P_{\mu^+} = -0.8$ and $P_{\mu^-} = +0.8$)

In Fig. 42, we compare predictions of the GPD model used in the previous section for H1 data to simulations of the BCA extraction at COMPASS using a muon beam of 100 GeV [25]. We present the comparison for one value of Q^2 (4 GeV^2) and two values of x_{Bj} (0.05 and 0.1). When we compute the BCA in the factorized exponential t dependence approximation, we find values compatible with zero, which are not represented in Fig. 42. Therefore, we just display the predictions of the model obtained in the non-factorized case using the same $\alpha' \sim 0.8$ GeV^{-2} value than in Ref. [28]. Both
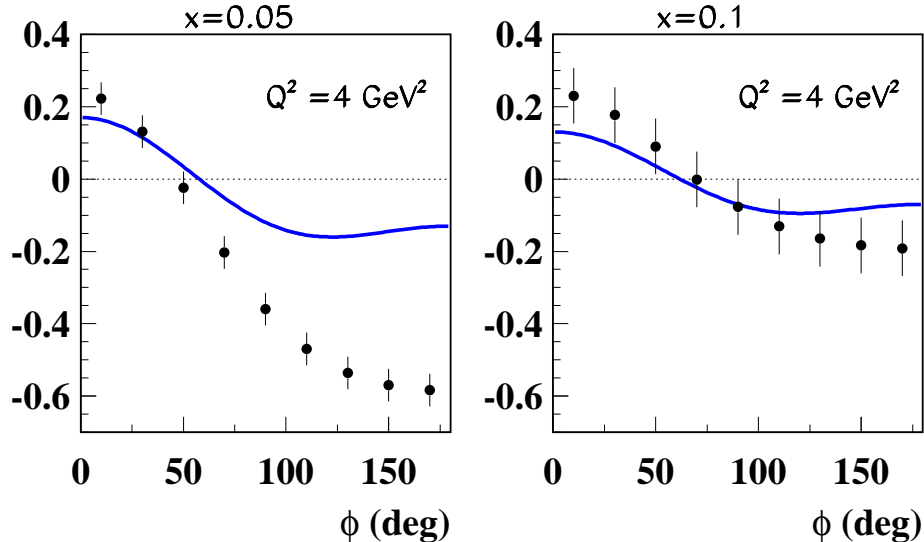
Fig. 42. Simulation of the azimuthal angular distribution of the beam charge asymmetry measurable at COMPASS at $E_\mu = 100$ GeV. We present the projected values and error bars in the range $|t| < 0.6$ GeV^2 for 2 values of x_{Bj} (0.05 and 0.1) at $Q^2 = 4$ GeV^2 (see Ref. [28]). The prediction of the GPD model with a non-factorized t dependence is shown (full line). The case of a factorized t dependence would lead to a prediction of the BCA compatible with zero and is not displayed.

the $\cos(\phi)$ and $\cos(2\phi)$ terms contribute to a significant level to the BCA at COMPASS, as illustrated in Fig. 42. We notice that our predictions do not match with the COMPASS simulation done with the model described in Ref. [28]. This is another illustration of the large discriminative power of this observable on GPDs parameterizations, even for identical t dependence input.

At HERA, we have also samples of data with electron and positron beams. Therefore, it has been possible to extract the beam charge asymmetry, $A_C = \frac{d\sigma^+/d\phi - d\sigma^-/d\phi}{d\sigma^+/d\phi + d\sigma^-/d\phi}$. A former pioneering measurement of the BCA at HERMES [26] is shown in Fig. 43. Then, recent results from HERMES [26] and H1 [19] are presented in Fig. 44 and 45, which correspond to $x_{Bj} \sim 0.1$ for HERMES and $x_{Bj} \sim 10^{-3}$ for H1. Note that in H1 we have kept a different convention in the definition of ϕ than in fixed target experiments, namely $\phi_{H1} = \pi - \phi_{HERMES}$. The advantage of the convention we have considered in H1 is that, a positive p_1 (with $BCA = p_1 \cos \phi$) means a positive real part of the DVCS amplitude. Both experiments show that the present
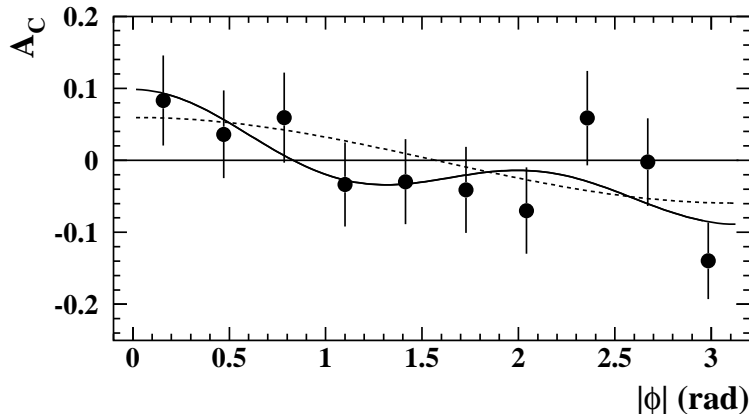
Fig. 43. Beam charge asymmetry A_C from HERMES data as a function of $|\phi|$. Statistical uncertainties are shown. The solid curve represents the four–parameter fit: $(-0.011 \pm 0.019) + (0.060 \pm 0.027)\cos\phi + (0.016 \pm 0.026)\cos 2\phi + (0.034 \pm 0.027)\cos 3\phi$. The dashed line shows the pure $\cos\phi$ dependence.

status of GPD models can correctly described the BCA measurements. In case of H1, factorized parameterizations of GPDs (in t) are the most simple choices compatible with measurements (see above), and for HERMES, the sensitivity of the hypothesis of the t-dependence is illustrated in Fig. 44. If we consider the overall description in Fig. 44, the factorized ansatz (without D-term) is favored by HERMES BCA measurements. The D-term is a part of some parameterizations of GPDs that is non-zero only in the ERBL domain. That's why BCA, which provides a sensitivity the real part of the DVCS amplitude, gets a sensitivity to this (unknown) term. In general also, the factorized ansatz is much more stable with respect to the D-term contribution, when compared to the non-factorized (Regge) ansatz. Indeed, the spread between Regge with/without D-term predictions is huge, whereas the D-term has only a small impact on the factorized predictions. As the D-term is almost completely unknown, it is interesting to make choice of parameterizations (if possible) that can reduce their sensitivity to it. In Ref. [26], it is mentioned that the Regge (without D-term) is favored, based on the observation of the t dependence. However, it is not that clear when considering all data points. In any case, the experimental results presented in Fig. 44 and 45 are the first obtained on BCA and then important pieces to provide constraints on the real part of the amplitude in future developments of GPDs phenomenology.

A specific analysis has been done in the H1 experiment concerning the real part of the DVCS amplitude [19]. From Eq. (13) and measurements of BCA and DVCS cross section, it is possible to extract the ratio of the real
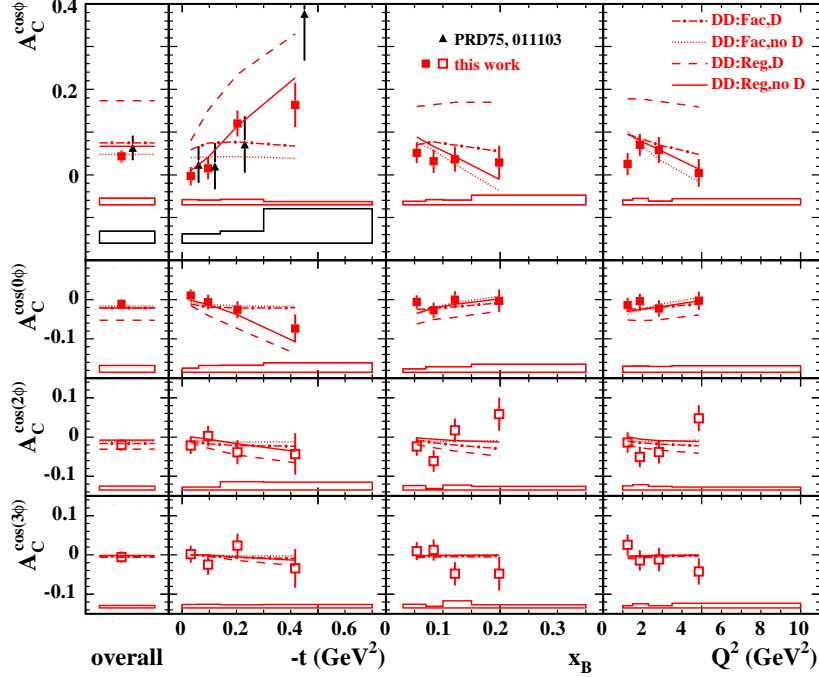
Fig. 44. Moments of the Beam charge asymmetry from HERMES data.

to imaginary parts of the DVCS amplitude

$$\rho = \mathrm{Re}A_{DVCS}/\mathrm{Im}A_{DVCS}.$$

This ratio is a key quantity which can also be derived through a dispersion relation, which takes a simple form in the high energy limit. Indeed, at low x_{Bj}, when the W dependence of the DVCS cross section is dominated by a single term in W^δ (with $\delta > 0.3$), the dispersion relation can be written as

$$\mathrm{Re}A_{DVCS}/\mathrm{Im}A_{DVCS} = \tan\left(\frac{\pi\delta(Q^2)}{8}\right), \tag{14}$$

where $\delta(Q^2)$ is the power governing the W dependence of the DVCS cross section at a given Q^2. As we have measured δ independently from DVCS cross sections only [19] (see previous section), we can compute this ratio, with the very reasonable assumption that the dispersion relation are correct. We obtain: $\rho = 0.25 \pm 0.06$. To be compared to the value extracted from BCA measurement and the subsequent extraction of p_1, which gives $\rho =$
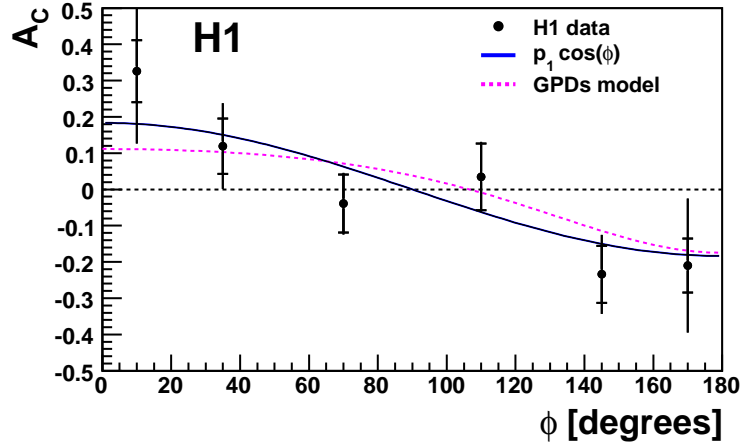
Fig. 45. Beam charge asymmetry as a function of ϕ from H1 data [19]. Note that the ϕ convention chosen in H1 is different from HERMES (see text). The inner error bars represent the statistical errors, the outer error bars the statistical and systematic errors added in quadrature. A fit in $p_1 \cos\phi$ is presented, where p_1 is a free parameter (full line), together with the GPDs model prediction (dashed line).

0.23 ± 0.08. Both values are found in good agreement. After this brief discussion, we can also understand simply how the sensitivity of the beam charge asymmetry observable is built with α'. The BCA is proportional to the ratio of real to imaginary part of the DVCS amplitude and this ratio can be expressed with respect to t as

$$\rho[t] = \mathrm{Re}A_{DVCS}/\mathrm{Im}A_{DVCS}[t] \simeq \mathrm{Re}A_{DVCS}/\mathrm{Im}A_{DVCS}[0](1 - \alpha'|t|).$$

Then, for small values of α', we do not expect much sensitivity of this ratio and thus of the BCA.

Regarding the kinematic coverage of fixed-target experiments (see Fig. 46), the Jefferson Lab (JLab) experiments play a major role in the field, exploring the large x_{Bj} and low Q^2 kinematic domain. JLab experiments can measure beam spin or target spin asymmetries [27] and then access directly the imaginary part of the DVCS amplitude in the valence domain. Of course, we can not exclude a priori that higher twists effects would completely spoil any perturbative treatment of the experimental results in this area. Below, we describe briefly few characteristic measurements at JLab related to GPDs physics.

An important recent result has been obtained by the Hall A E-00-110

experiment [27], which demonstrates that measurements at JLab are mainly dominated by leading twists contributions. It is shown in Fig. 47. From the observed Q^2 scaling of the imaginary part of the DVCS amplitude (see Fig. 47) this result provides an indication that the measurement of the imaginary part of the DVCS amplitude follows a typical Bjorken scaling, observed over the Q^2 range covered by the experiment. Which means that leading twists terms are likely to dominate. Of course, the range in Q^2 accessible is not large but the the high precision of the data makes this last statement quite reasonable. An upgrade at larger energies of the lepton beam is obviously an important issue to get a sensitivity to higher Q^2 values (and larger W).
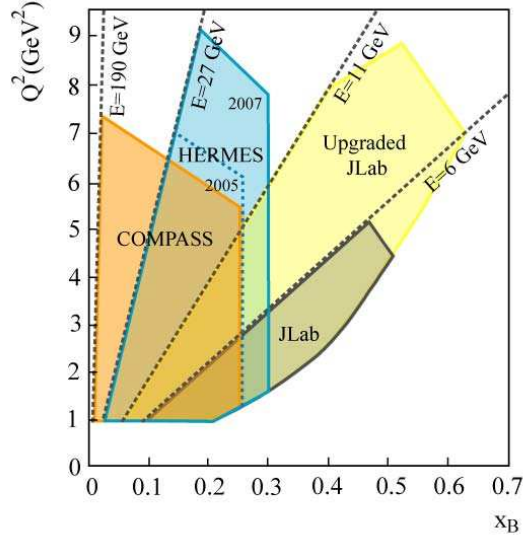

Fig. 46. Kinematic coverage for fixed-target experiments: (i) COMPASS at 190 GeV; (ii) HERMES at 27.6 GeV, dotted line for existing data ($\leq$ 2005), solid line for future (2005-2007) data with an integrated luminosity higher by about one order of magnitude; (iii) JLAB experiments at 6 GeV, and at 11 GeV (after upgrade).

Apart from DVCS/BH interference measurements, a separation between BH and DVCS processes has been obtained with the Hall A E-00-110 experiment. The measurement of the 4-fold (polarized and unpolarized) differential cross sections $\frac{d\sigma}{dx_B dQ^2 dt d\phi}$ (for the real photon production process) has been done for three values of Q^2(in the kinematic domain $W \approx 2$ GeV and $x > 0.1$). Results are shown in Fig. 48 for $< Q^2 >=$2.3 GeV^2 [27]. The particular shape in ϕ of the unpolarized cross section (Fig. 48) is typical of the BH process. The dot-dot-dashed curve in Fig. 48 shows its precise
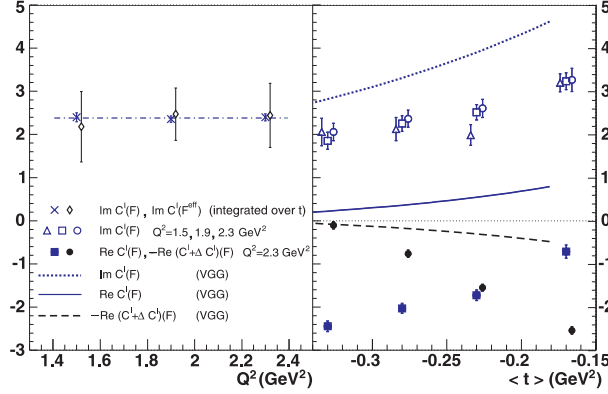
Fig. 47. Q^2 dependence of imaginary part of the DVCS amplitude (left). We observe a scaling over the range in Q^2 covered by the analysis.
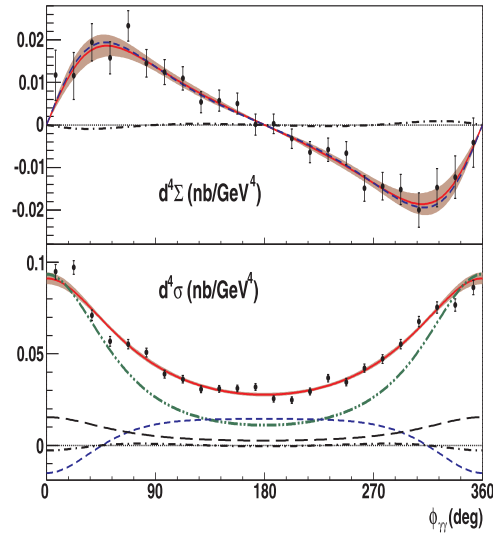
Fig. 48. Difference of (beam) polarized cross sections for DVCS on the proton, as a function of the Φ angle, measured by the JLab Hall A collaboration. The average kinematics is $< x_{Bj} >$=0.36, $< Q^2 >$=2.3 GeV^2 and $< -t >$=0.28 GeV^2. The figure on the bottom shows the total (i.e unpolarized) cross section as a function of Φ. The BH contribution is represented by the dot-dot-dashed curve.

shape and contribution. It can be seen that it dominates most of the cross sections and, only around $\Phi = 180^o$, there is a large discrepancy (a factor ≈ 2) between the BH and the data which could be attributed to the DVCS

process itself.

Fig. 49. Left: kinematic coverage and binning in the (x_B, Q^2) space. Right: Beam spin asymmetry $A(\phi)$ for 2 of the 62 $(x_B, Q^2, t)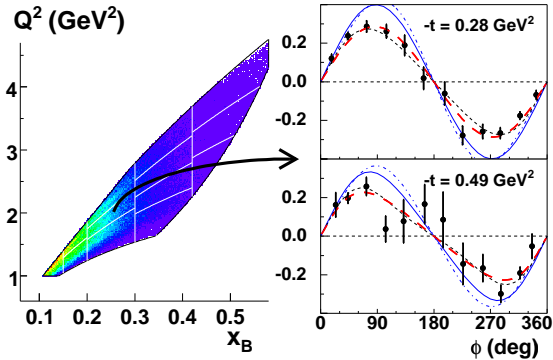$ bins, corresponding to $\langle x_B \rangle = 0.249$, $\langle Q^2 \rangle = 1.95$ GeV^2, and two values of $\langle t \rangle$. The long-dashed curves correspond to fits with $A = \frac{a \sin \phi}{1 + c \cos \phi}$. The dashed curves correspond to a Regge calculation. GPDs calculations are also shown as full lines.

Let us present a final measurement from the (JLab) Hall B E-00-113 experiment, concerning beam spin asymmetries (BSAs) [27], which shows (again) clearly the interest for an upgrade at larger energies. Results are presented in Fig. 49 with GPDs or Regge (non-perturbative) models. The asymmetries are fitted according to the relation

$$A = \frac{a \sin \phi}{1 + c \cos \phi + d \cos 2\phi} \tag{15}$$

and extracted values of a are displayed in Fig. 50. As can be seen in Fig. 50, the discrimination of Regge (soft) or GPDs (hard) approaches is not conclusive from the present data. Therefore, the upgrade with 12 GeV electrons is very interesting to address this separation between soft and hard physics at JLab.

A final comment is in order concerning the measurement of asymmetries (from DVCS/BH interference) in fixed target experiments. Experiments at JLab and data collected by HERMES allow to determine transverse target-spin asymmetries, by controlling the polarization of the target. This will be a possibility of the future COMPASS project described above. Experimentally, we need to introduce another azimuthal angle ϕ_S to characterize completely the events measured in such configurations, where ϕ_S represents the direction of the spin of the target with respect to the plane of the leptons (incident and scattered). The great interest is then that the $\cos \phi$ moment
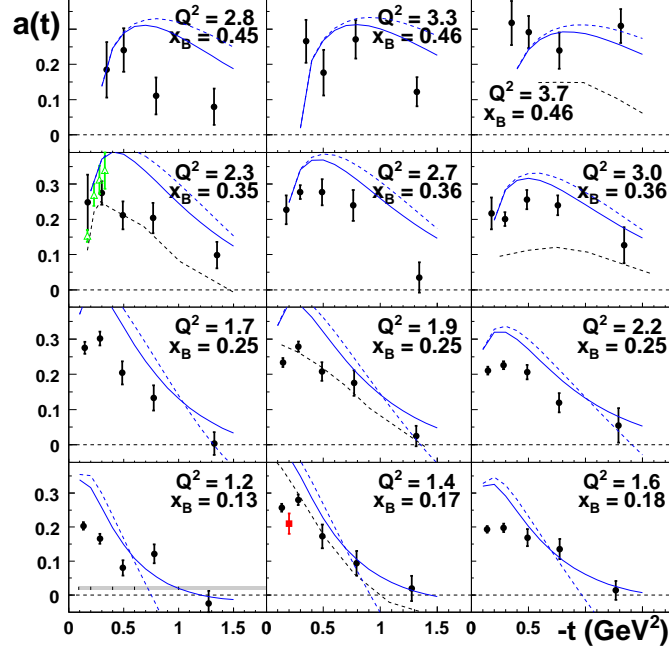
Fig. 50. Extracted values a of the DVCS-BH interference as measured in a spin asymmetry, with $A = \frac{a \sin \phi}{1 + c \cos \phi + d \cos 2\phi}$. They are shown as a function of $-t$ for different bins in (x_B, Q^2). The solid curves represent a GPD model and the dashed curves a Regge approach.

of the asymmetry $d\sigma(\phi, \phi_S) - d\sigma(\phi, \phi_S + \pi)$ is proportional to the imaginary part of GPDs of types H and E. Remind the short note we have written in the last section: the contribution of GPDs of type E are damped by kinematic factors of orders $|t|/M_p^2$ in all the observables we have discussed till now. This is not the case for transverse target-spin asymmetries. Therefore, these measurements are particularly interesting in the quest for GPDs. The strong interest in determining GPDs of type E is that these functions appear in a fundamental relation between GPDs and angular momenta of partons. Indeed, GPDs have been shown to be related directly to the total angular momenta carried by partons in the nucleon, via the Ji relation [22]

$$\frac{1}{2} \int_{-1}^{1} dx\, x \left(H_q(x, \xi, t) + E_q(x, \xi, t) \right) = J_q. \qquad (16)$$

As GPDs of type E are essentially unknown apart from basic sum rules, any improvement of their knowledge is essential. From Eq. (16), it is clear that

we could access directly to the orbital momentum of quarks if we had a good knowledge of GPDs H and E. Indeed, J_q is the sum of the longitudinal angular momenta of quarks and their orbital angular momenta. The first one is relatively well known through global fits of polarized structure functions. It follows that a determination of J_q can provide an estimate of the orbital part of its expression. In Ji relation (Eq. (16)), the function H is not a problem as we can take its limit at $\xi = 0$, where H merges with the PDFs, which are well known. But we need definitely to get a better understanding of E. First measurements of transverse target-spin asymmetries have been realized at JLab [27] and HERMES [26]. We present results obtained by HERMES [26] in Fig. 51. The typical sensitivity to hypothesis on J_q values is also illustrated in Fig. 51, with the reserve that in this analysis, the observed sensitivity to J_q is model dependent. Then, it is just a first step, very challenging from the experimental side. Certainly, global fits of GPDs (if possible) would give a much more solid (less model dependent) sensitivity to J_q.

In order to give more intuitive content to the Ji relation (16), we can comment further its dependence in the function E. From our short presentation of GPDs, we know that functions of type E are related to matrix elements of the form $\langle p', s' | \mathcal{O} | p, s \rangle$ for $s \neq s'$, which means helicity flip at the proton vertex ($s \neq s'$). That's why their contribution vanish in standard DIS or in processes where t tends to zero. More generally, their contribution would vanish if the proton had only configurations where helicities of the partons add up to the helicity of the proton. In practice, this is not the case due to angular momentum of partons. This is what is reflected in a very condensed way in the Ji relation (Eq. (16)). Then, we get the intuitive interpretation of this formula: it connects E with the angular momentum of quarks in the proton. A similar relation holds for gluons [22], linking J_g to H_g and E_g and both formulae, for quarks and gluons, add up to build the proton spin

$$J_q + J_g = 1/2.$$

This last equality must be put in perspective with the asymptotic limits for J_q and J_g at large scale Q^2, which read $J_q \to \frac{1}{2} \frac{3n_f}{16+3n_f}$ and $J_g \to \frac{1}{2} \frac{16}{16+3n_f}$, where n_f is the number of active flavors of quarks at that scale (typically $n_f = 5$ at large scale Q^2) [22]. In words, half of the angular momentum of the proton is carried by gluons (asymptotically). It is not trivial to make quantitative estimates at medium scales, but it is a clear indication that orbital angular momentum plays a major role in building the angular momentum of the proton. It implies that all experimental physics issues that intend to access directly or indirectly to GPDs of type E are essential in the understanding of the proton structure, beyond what is relatively well
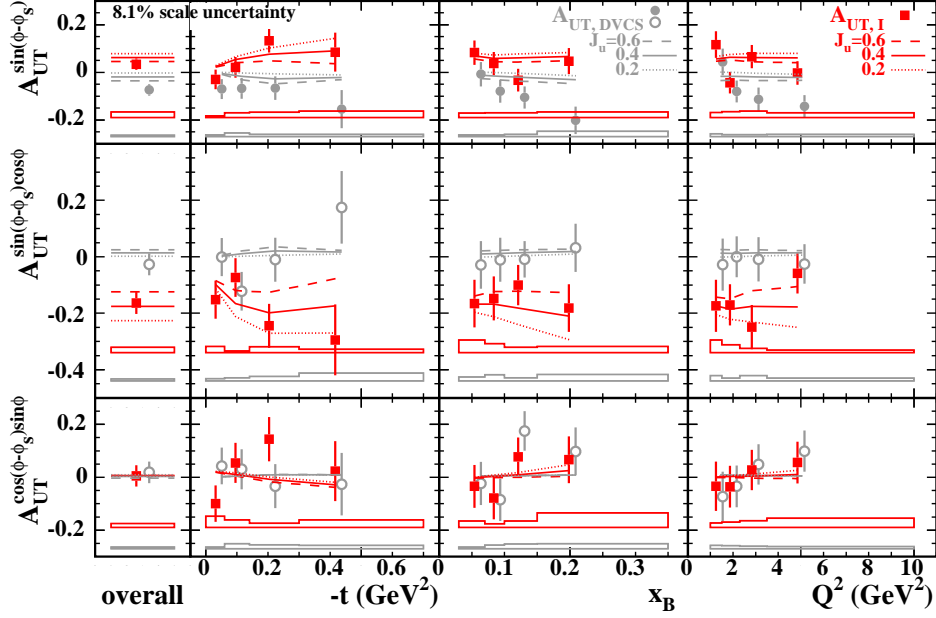
Fig. 51. Target-spin asymmetry amplitudes describing the dependence of the squared DVCS amplitude (circles, $A_{UT,DVCS}$) and the interference term (squares, $A_{UT,I}$) on the transverse target polarization. In the notations, U refers to Unpolarized beam and T to Transversely polarized target. The circles (squares) are shifted right (left) for visibility. The curves are predictions of a GPD model with three different values for the u-quark total angular momentum J_u and fixed d-quark total angular momentum $J_d = 0$ (see [26]). This is a first important (model dependent) check of the sensitivity these data to the Ji relation.

known concerning its longitudinal momentum structure in x_{Bj}. And that's also why first transverse target-spin asymmetries (which can provide the best sensitivity to E) are so important and the fact that such measurements have already been done is promising for the future.

Clearly, we understand at this level the major interest of GPDs and we get a better intuition on their physics content. They simultaneously probe the transverse and the longitudinal distribution of quarks and gluons in a hadron state and the possibility to flip helicity in GPDs makes these functions sensitive to orbital angular momentum in an essential way. This is possible because they generalize the purely collinear kinematics describing the familiar twist-two quantities of the parton model. This is obviously illustrating a fundamental feature of non-forward exclusive processes.

11. Outlook

In this habilitation thesis document, the idea is to cover the main advances in (hard) diffraction during the last years for which our impact was significant, either from the experimental side or, when possible, from the interpretation border.

Concerning inclusive diffraction, we have discussed the main areas in which we have contributed: measurements, extraction of diffractive PDFs, HERA results put in perspective with Tevatron observables, prospectives for LHC. We have discussed in length a very important aspect that makes diffraction in DIS so interesting at low x_{Bj}: its interpretation in the dipole formalism and its connection to saturation effects. Indeed, diffraction in DIS has appeared as a well suited process to analyze saturation effects at large gluon density in the proton. In the dipole model, it takes a simple and luminous form, with the introduction of a saturation scale Q_s. Diffraction is then dominated by dipoles of size $r \sim 1/Q_s$, which makes naturally diffractive processes sensitive to saturation effects. In particular, it provides a simple explanation of the constance of the ratio of diffractive to total cross sections as a function of W (at fixed Q^2 values). During the last three years, we had several opportunities to present these results in plenary talks [29, 30, 31].

Concerning exclusive processes and DVCS, our contributions have been dominant in the experimental measurements, in particular with determinations of DVCS cross sections and their dependences in t (analyzing H1 data). These measurements have allowed us to merge DVCS with other exclusive reactions at HERA and to provide a common perspective for all processes. For example, with results of the energy dependence power, $\delta(Q^2)$ with $\sigma \sim W^{\delta}$, and of the exponential t slope, $b(Q^2, W)$, with $d\sigma/dt \sim e^{-b|t|}$. A unified picture is clear. Either from the dipole approach of in the GPDs formalism. Of course, both approaches include the same main physics features, either in the dipole cross section (dipole formalism) of in the initial conditions (GPDs formalism). A specific interest for DVCS is important: DVCS is certainly the best candidate for a (pure) description with GPDs, avoiding unknowns from the vector meson wave functions. Along the years and analysis, we have focused our attention, not only on HERA results but also on all the other experiments measuring DVCS or exclusive (hard) particle production. This perspective gives much more insight into the definition of key elements for the future. This explains why we have been interested in the COMPASS project for measuring DVCS at CERN after 2010. The expected kinematic domain is lying between H1/ZEUS and HERMES/JLab experiments. It gives promising perspectives in understanding the transition from low to large x_{Bj} for many observables. Our experimental work on

the impact parameter dependence of parton distributions (also as a function of x_{Bj}) is of fundamental interest. It provides a completely new information on the spatial extension of partons inside the proton (or hadrons). We have explained the new insights of such analysis. For example, our measurements have established that small x_{Bj} partons of the nucleon contribute more for large values of b. Also, shadowing of small x_{Bj} parton distributions, is probably stronger at small values of b since partons in the geometric center of the nucleon are more effectively shielded by the surrounding partons. These and many other results and intuitive pictures for the parton structure of hadrons give rise to (first) predictions for the impact parameter dependence of GPDs that reflect the underlying microscopic dynamics.

Of course, we do not forget that the dependence of GPDs on three kinematical variables, and the number of distributions describing different helicity combinations present a considerable complexity. In a sense this is the price to pay for the amount of physics information encoded in these quantities. It is however crucial to realize that for many important aspects one need not fully disentangle this complexity. The relation of longitudinal and transverse structure of partons in a nucleon, or of nucleons in a nucleus, can be studied quantitatively from the distribution in the two external kinematical variables ξ and t, even if the deconvolution of the loop integral over the variable x is not performed. We have developed in length this aspect in this review. We had some opportunities to present these results and ideas in plenary talks during the last years [32, 33].

REFERENCES

[1] H. Abramowicz and A. Caldwell, Rev. Mod. Phys. **71** (1999) 1275.

[2] M. Derrick *et al.* [ZEUS Collaboration], Z. Phys. C **68** (1995) 569; C. Adloff *et al.* [H1 Collaboration], Z. Phys. C **76** (1997) 613.

[3] S. Chekanov *et al.* [ZEUS Collaboration], Eur. Phys. J. **C38** (2004) 43; S. Chekanov et al. [ZEUS Collaboration], Nucl. Phys. **B713** (2005) 3; A. Aktas *et al.* [H1 Collaboration], Eur. Phys. J. C **48** (2006) 715; A. Aktas *et al.* [H1 Collaboration], Eur. Phys. J. C **48** (2006) 749; E. Sauvan, Published in Tsukuba 2006, Deep inelastic scattering 211-214, arXiv:hep-ex/0607038; S. Chekanov [ZEUS Collaboration], Nucl. Phys. B **800** (2008) 1.

[4] J. C. Collins, Phys. Rev. D **57** (1998) 3051 [Erratum-ibid. D **61** (2000) 019902].

[5] G. Ingelman and P. E. Schlein, Phys. Lett. B **152** (1985) 256.

[6] L. Schoeffel, Nucl.Instrum.Meth. **A423** (1999) 439; C. Royon, L. Schoeffel, J. Bartels, H. Jung and R. B. Peschanski, Phys. Rev. D **63** (2001) 074004; J. Lamouroux, R. B. Peschanski, C. Royon and L. Schoeffel, Nucl. Phys. B **649** (2003) 312; C. Royon, L. Schoeffel, R. B. Peschanski and E. Sauvan, Nucl. Phys. B **746** (2006) 15; C. Royon, L. Schoeffel, S. Sapeta, R. B. Peschanski and E. Sauvan, Nucl. Phys. B **781** (2007) 1.

[7] CDF Collaboration, Phys. Rev. Lett. **84** (2000) 5043; Phys. Rev. Lett. **87** (2001) 141802.

[8] C. Royon, Acta Phys. Polon. B **37** (2006) 3571 [hep-ph/0612153].

[9] FP420 Coll., see http://www.fp420.com; AFP TDR in ATLAS to be submitted; see: http://project-rp220. web.cern.ch/project-rp220/index.html; C. Royon, preprint arXiv:0706.1796, proceedings of 15th International Workshop on Deep-Inelastic Scattering and Related Subjects (DIS2007), Munich, Germany, 16-20 Apr 2007.

[10] A.H. Mueller, Nucl. Phys. **B335** (1990) 115; N.N. Nikolaev and B.G. Zakharov, Zeit. für. Phys. **C49** (1991) 607.

[11] A. Bialas and R. Peschanski, Phys. Lett. **B378** (1996) 302; Phys. Lett. **B387** (1996) 405; H. Navelet, R. Peschanski, C. Royon, S. Wallon, Phys. Lett. B **385** (1996) 357; H. Navelet, R. Peschanski, C. Royon, Phys. Lett. B366 (1996) 329; A. Bialas, R. Peschanski, C. Royon, Phys. Rev. D **57** (1998) 6899; S. Munier, R. Peschanski, C. Royon, Nucl. Phys. B **534** (1998) 297.

[12] C. Marquet, R. B. Peschanski and G. Soyez, Nucl. Phys. A **756** (2005) 399; C. Marquet, R. B. Peschanski and G. Soyez, Phys. Rev. D **76** (2007) 034011.

[13] K. J. Golec-Biernat and M. Wusthoff, Phys. Rev. D **59** (1999) 014017; K. J. Golec-Biernat and M. Wusthoff, Phys. Rev. D **60** (1999) 114023; J. Bartels, K. J. Golec-Biernat and H. Kowalski, Phys. Rev. D **66** (2002) 014001; K. Golec-Biernat and S. Sapeta, Phys. Rev. **D74** (2006) 054032.

[14] C. Marquet and L. Schoeffel, Phys. Lett. B **639** (2006) 471.

[15] J. Breitweg et al. [ZEUS Collaboration], Eur. Phys. J. **C 2**, 2 (1998); M. Derrick et al. [ZEUS Collaboration], Eur. Phys. J. **C 6**, 603 (1999); C. Adloff

et al. [H1 Collaboration], Eur. Phys. J. **C 13**, 371 (2000); S. Chekanov *et al.* [ZEUS Collaboration], PMC Phys. A **1** (2007) 6.

[16] C. Adloff et al. [H1 Collaboration], Phys. Lett. **B 483**, 360 (2000); S. Chekanov et al. [ZEUS Collaboration], Nucl. Phys. **B 718**, 3 (2005).

[17] S. Chekanov et al. [ZEUS Collaboration], Nucl. Phys. **B 695**, 3 (2004); A. Aktas et al. [H1 Collaboration], Eur. Phys. J. **C 46**, 585 (2006).

[18] J. Breitweg *et al.* [ZEUS Collaboration], Phys. Lett. B **437** (1998) 432; C. Adloff *et al.* [H1 Collaboration], Phys. Lett. B **483** (2000) 23.

[19] C. Adloff *et al.* [H1 Collaboration], Phys. Lett. B **517** (2001) 47; A. Aktas *et al.* [H1 Collaboration], Eur. Phys. J. C **44** (2005) 1; F. D. Aaron *et al.* [H1 Collaboration], Phys. Lett. B **659** (2008) 796. L. Schoeffel, proceedings of the 15th International Workshop on Deep-Inelastic Scattering and Related Subjects (DIS2007), arXiv:0705.2925 [hep-ph].

[20] P. R. B. Saull [ZEUS Collaboration], arXiv:hep-ex/0003030; S. Chekanov *et al.* [ZEUS Collaboration], Phys. Lett. B **573** (2003) 46; S. Chekanov *et al.* [ZEUS Collaboration], arXiv:0812.2517 [hep-ex].

[21] M. Diehl, Eur. Phys. J. C **25** (2002) 223 [Erratum-ibid. C **31** (2003) 277]; M. Burkardt, Int. J. Mod. Phys. A **18** (2003) 173; A. V. Belitsky, X. d. Ji and F. Yuan, Phys. Rev. D **69** (2004) 074014; L. Frankfurt, M. Strikman and C. Weiss, Ann. Rev. Nucl. Part. Sci. **55** (2005) 403.

[22] X. D. Ji, Phys. Rev. Lett. **78** (1997) 610; Phys. Rev. **D55** (1997) 7114; M. Diehl, T. Gousset, B. Pire and J. P. Ralston, Phys. Lett. B **411** (1997) 193; L. L. Frankfurt, A. Freund and M. Strikman, Phys. Rev. D **58** (1998) 114001 [Erratum-ibid. D **59** (1999) 119901]; A. V. Belitsky, D. Mueller and A. Kirchner, Nucl. Phys. B **629** (2002) 323; M. Diehl, Phys. Rept. **388**, 41 (2003); A. V. Belitsky and A. V. Radyushkin, Phys. Rept. **418**, 1 (2005).

[23] K. Kumerički, D. Mueller and K. Passek-Kumerički, Eur. Phys. J. C **58** (2008) 193.

[24] M. Diehl, T. Feldmann, R. Jakob and P. Kroll, Eur. Phys. J. C **39** (2005) 1.

[25] L. Schoeffel, Phys. Lett. B **658** (2007) 33.

[26] A. Airapetian *et al.* [HERMES Collaboration], Phys. Rev. Lett. **87** (2001) 182001; A. Airapetian *et al.* [HERMES Collaboration], Phys. Rev. D **75** (2007) 011103; A. Airapetian *et al.* [HERMES Collaboration], JHEP **0806** (2008) 066.

[27] S. Stepanyan *et al.* [CLAS Collaboration], Phys. Rev. Lett. **87** (2001) 182002. C. Munoz Camacho *et al.* [Jefferson Lab Hall A Collaboration and Hall A DVCS Collaboration], Phys. Rev. Lett. **97** (2006) 262002; S. Chen *et al.* [CLAS Collaboration], Phys. Rev. Lett. **97** (2006) 072002; F. X. Girod *et al.* [CLAS Collaboration], Phys. Rev. Lett. **100** (2008) 162002;

[28] N. d'Hose et al., Nucl. Phys. A **711** (2002) 160.

[29] L. Schoeffel, *Diffractive cross sections at HERA and diffractive PDFs*, published in the proceedings of Ringberg Workshop on New Trends in HERA Physics 2008 (Ringberg Castle, Tegernsee, Germany, 5-10 Oct 2008), arXiv:0811.3142 [hep-ph].

[30] L. Schoeffel, *Review of diffraction at HERA and Tevatron*, published in the proceedings of Photon 2007 (Paris, France, 9-13 Jul 2007), Nucl.Phys.Proc.Suppl.184:81-84,2008.

[31] L. Schoeffel, *Diffraction: Recent results and implications for LHC*, published in the proceedings of the 42nd Rencontres de Moriond on QCD and Hadronic Interactions (La Thuile, Italy, 17-24 Mar 2007), arXiv:0705.1413 [hep-ph].

[32] L. Schoeffel, *Deeply Virtual Compton Scattering at HERA and perspectives at CERN*, published in the proceedings of 6th International Conference on Perspective in Hadronic Physics (Trieste, Italy, 12-18 May 2008), AIP Conf.Proc.1056:372-379,2008.

[33] L. Schoeffel, *QCD analysis of diffractive phenomena*, published in the proceedings of 27th International Conference on Physics in Collision -PIC 2007- (Annecy, France, 26-29 Jun 2007), Acta Phys.Polon.Supp.1:379-388,2008.